Biomass and Bioenergy 108 (2018) 398–414

Contents lists available at ScienceDirect

Biomass and Bioenergy

journal homepage: www.elsevier.com/locate/biombioe

Research paper

Simple pyrolysis experiments for the preliminary assessment of biomass feedstocks and low-cost tar cracking catalysts for downdraft gasification applications

Matthew E. Boot-Handford[a,*], Elaine Virmond[b], Nick H. Florin[c,d], Rafael Kandiyoti[a], Paul S. Fennell[a,**,1]

[a] Department of Chemical Engineering, Imperial College London, SW7 2AZ, United Kingdom
[b] Universidade Federal de Santa Catarina, Departamento de Engenharia Química e Engenharia de Alimentos, Campus Florianópolis, Brazil
[c] Grantham Institute for Climate Change, Imperial College London, SW7 2AZ, United Kingdom
[d] Institute for Sustainable Futures, University of Technology Sydney, NSW 2007, Australia

ABSTRACT

The pyrolysis behaviour of beech wood, two rice husk variants from Brazil (BRH) and Thailand (TRH) and a solid waste water treatment residue from textile manufacture (TIR) were investigated using a lab-scale, 2-stage fixed-bed reactor at 773 K. Char yields increased and volatile yields decreased with increasing ash content. The TRH released 40% less tar than the BRH which was attributed to the substantially higher potassium content of the Thai species. The combustion reactivity of the TRH char in air at 773 K was similar to the BW char and almost double the reactivity of the BRH and TIR chars. The BW and TRH chars had a greater volume of macropores indicating that char combustion occurs predominantly through the growth and extension of the macroporous pore network. A different trend was observed for the char gasification reactivity with CO_2 at 1173 K. The Ca and Mg content of the chars were found to have a more important catalytic role in the char gasification reactions with CO_2.

The effect of exposing volatile products from beech wood pyrolysis to elevated temperatures (973–1173 K) and sand beds containing calcined limestone or dolomite in a simulated downdraft gasification environment was also investigated. Tar yields decreased after exposure to elevated temperature and calcined limestone or dolomite. Tar cracking favoured the production of CO. CO yields were between 22 and 23 wt% at 1173 K. Calcined dolomite was slightly more effective at cracking tar than calcined limestone, eliminating 98 wt% of the tar at 1173 K.

1. Introduction

Biomass utilisation has received renewed interest over recent years in response to growing concerns over volatile fossil fuel prices, energy security, and climate change [1]. Biomass is widely considered to be a renewable source of energy which is often available in large quantities and at a low cost as a by-product of agriculture and forestry. Gasification offers one of the most efficient and flexible methods for processing biomass, providing a means to convert 60–90% of the energy content of the biomass into a versatile syngas containing both useful (H_2 + CO) and problematic products such as tar [2].

Tar is operationally defined as any organic material in the product stream that is condensable in the gasifier, downstream processing steps or conversion devices [3]. Biomass tar typically includes long-chain aliphatic hydrocarbons, single ring to 5-ring aromatic compounds along with other oxygen-containing hydrocarbons and complex polycyclic-aromatic hydrocarbons (PAHs) [4]. The presence of tar in syngas from biomass gasification can lead to a number of downstream operational issues; it is particularly problematic for advanced technologies such as fuel cells that have very low tolerances of < 80 ppb tar contamination [3].

Downdraft gasifiers are a class of fixed bed reactor that are particularly suited to applications of small scale, decentralised electricity and heat production [2,5]. They are relatively simple and cheap to

* Corresponding author.
** Corresponding author.
E-mail addresses: m.boot-handford@imperial.ac.uk (M.E. Boot-Handford), p.fennell@imperial.ac.uk (P.S. Fennell).
[1] Currently visiting the Department of Chemical and Biological Engineering, University of British Columbia.

https://doi.org/10.1016/j.biombioe.2017.10.048
Received 6 December 2016; Received in revised form 25 October 2017; Accepted 30 October 2017

construct and easy to maintain and operate when compared with more complex technologies such as those based on a fluidised bed concept. Dowdraft gasifiers are also the most efficient gasifier concept for eliminating tar species. Over the past few decades, hundreds to thousands of small scale fixed-bed biomass gasifiers have been installed throughout China and India ranging in capacity from a few kW to 10 and even 50 MW for the purpose of rural electrification, albeit with limited success [6,7]. The primary obstacle limiting successful deployment of small-scale biomass gasification technology concerns the cost and added process complexity associated with controlling tar emissions.

Hot gas conditioning via catalytic cracking is one of the most effective techniques for the removal of tars [4,8–10]. Tar cracking/reforming catalysts can be added directly to a gasifier as a bed material in the case of a fluidised bed gasifier (primary catalyst); or to a secondary reactor downstream of the gasifier for syngas upgrading and tar elimination (secondary catalyst). Catalysts based on nickel and other noble metals such as Rh, Pd, Pt and Ru have proven to be highly effective [11–15]. However the expense and high toxicity typically associated with these types of catalyst means that they are less feasible when considering deployment of gasification technology for providing small-scale, decentralised electrification and fuel production in rural, geographically isolated locations with access to large quantities of agricultural or forestry waste such as rice and timber mills. An alternative class of catalysts more suited to such applications are inexpensive natural mineral based gas conditioning catalysts such as dolomite, magnesite and olivine [16–23].

Calcined dolomites have been well studied as tar cracking catalysts for biomass gasification applications [23–27]. Delgado and Aznar et al. compared the catalytic tar cracking activity of calcite, magnesite and dolomite in their calcined forms for downstream conditioning of syngas produced from steam gasification of biomass [28]. Calcined dolomite proved to be the most effective followed by MgO and CaO. Tar cracking favoured the production of permeant gases (e.g. CO, H_2 CO_2 etc) with tar cracking over calcined dolomite producing the highest gas yields. In a later paper, Corrella et al. investigated the in-bed tar cracking catalytic activity of calcined dolomite with both untreated olivine and olivine treated with Ni [29]. The tar content of the gas exiting the gasifier had 60% less tar when calcined dolomite was used as the in-bed additive compared with tests using Ni treated olivine. However, the authors note that calcined dolomite suffered from significant fragmentation and attrition resulting in the production of 4–6 times more fines than when olivine was used as an in-bed additive. Similar behaviour has been reported elsewhere [23,30,31]. Devi et al. studied the effects of sand, untreated olivine and calcined dolomite in a secondary reactor downstream of a biomass gasifier on the yields of GC-detectable tar species [32]. The calcined dolomite reduced the total amount of heavy polyaromatic hydrocarbons (PAHs) by 90% and the total amount of tar in the syngas from 4 gm^{-3} to 1.5 gm^{-3}.

The first part of this paper describes and discusses results from simple biomass pyrolysis experiments conducted using a single-stage fixed bed reactor. Used in this way, the reactor allows for high throughput, preliminary investigations into the suitability of potential biomass feedstocks for gasification processes. The results provide information pertaining to the influence of inherent biomass properties on the thermochemical breakdown of a prospective biomass gasifier feed.

The second strand of this research made use of the reactor in its two-stage configuration. The 2-stage reactor concept was designed for studying tar cracking interactions in a simulated downdraft gasification environment where the first reactor stage was operated as the pyrolysis zone and the 2nd stage as the combustion and/or gasification zone where tar cracking takes place [33]. The types of interaction that take place in the 2nd stage depends on the temperature, presence of 2nd stage packing material and gas composition added through the 2nd stage gas inlet (which simulates the throat section of a dowdraft gasifier).

Here we investigate the potential of calcined dolomite and limestone as (primary) tar cracking catalysts for downdraft gasification applications where the minerals could be added with the feed to reduce tar emissions and eliminate the need for secondary downstream tar removal. Calcined limestone is often discounted as a tar cracking catalyst for in-bed use in fluidised bed gasification processes due to concerns relating to particle sintering and agglomeration leading to more rapid catalyst deactivation and/or de-fluidisation [34]. This behaviour presents less of a problem when considering the use of CaO as a single pass catalyst in a downdraft gasification process. Furthermore, calcined limestone offers the benefit that it could be employed as a CO_2 sorbent for sorbent enhanced water-gas shift (SEWGS), sorbent enhanced reforming (SER) and carbon capture and storage (CCS) applications [31,35,36]. The addition of lime has also been found to prevent the formation of low melting point, alkali metal silicate eutectic salts that can lead to slagging and bed agglomeration issues, which can be particularly problematic when handling biomass varieties containing large amounts of ash [37].

2. Experimental

2.1. Reactor

A detailed description of the development and operation of the 2-stage reactor used for this study and its use and limitations in the study of tar production and cracking has been reported in a number of previous publications [33,38–44] and will be described only briefly here. The version of the reactor employed in this work is the same as that described by Kandiyoti et al. [33] and Dabai et al. [43] (Fig. 1).

The first stage of the reactor consisted of a stainless-steel tube (12 mm ID, 2 mm wall thickness), 200 mm in length with a welded flange connection at its base to allow for connection to the 2nd reactor stage or tar trap. The 1st stage gas supply and thermocouple were introduced through a twin-ferrule compression fitting connection at the top of the stage. Before each experimental run, 1 g of biomass (106–150 μm) was loaded into the 1st stage and supported in position with a strip of stainless steel wire mesh.

The 2nd stage was constructed from an Incoloy 800 HT tube (12 mm ID, 2 mm wall thickness), 150 mm in length with welded top and bottom flanges. The top flange was specially designed to incorporate three equally spaced, lateral gas inlets that enabled the gas velocity and composition through the 2nd stage to be varied independently of the 1st stage. The 2nd stage temperature was controlled via a thermocouple inserted through a spigot welded to the outside of the reactor stage.

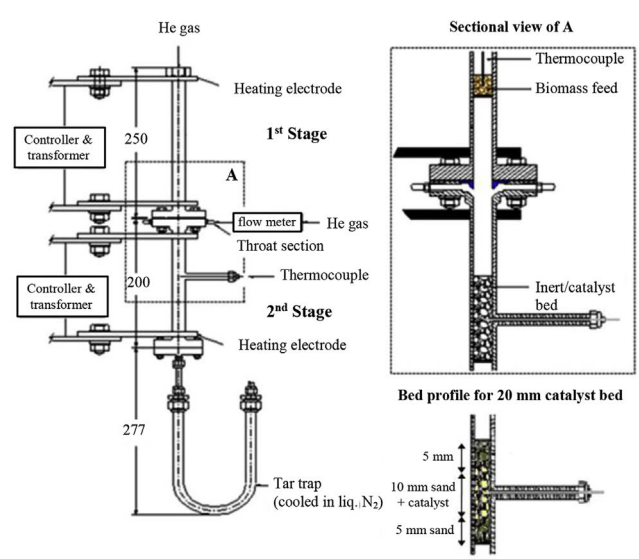

Fig. 1. Diagram of the 2-stage, fixed-bed reactor, reproduced from Monteiro Nunes et al. [41].

When investigating the effect of the different solids on the tar yield, 20 mm beds comprised of a 10 mm section of either 20 wt% limestone or 20 wt% dolomite (355–425 μm) mixed with 80 wt% sand (500–710 μm) positioned between two 5 mm sections of sand were loaded into the 2nd stage prior to assembly. The beds were held in position with a wire mesh plug.

The tar trap was a stainless-steel U-tube (12 mm ID, 2 mm wall thickness) fitted with a stainless steel flange for connecting to the 1st or 2nd reactor stage. The tar trap was submerged in a liquid nitrogen bath for the duration of the experiment to condense tar and other volatile products for analysis. The exit of the trap was packed with wire mesh to enhance the internal surface area of the tar trap ensuring efficient trapping of the volatile products in the form of aerosol droplets.

The reactor was heated via four copper electrodes attached to the outside of the reactor body at the top and bottom of the two stages. The reactor body acted as a resistance heater. The top electrode was rigid and doubled up as a mount for the reactor. The other three electrodes were attached to the reactor with flexible woven copper cables to allow for thermal expansion of the reactor body.

2.1.1. Materials

The biomass and waste samples investigated in this study were a beech wood from Germany (BW), a rice husk originating from Brazil (BRH), a rice husk originating from Thailand (TRH) and a dried solid residue (sludge) obtained from waste water treatment at a textile manufacturing facility in Brazil (Textile Industry Residue, TIR). Biomass samples were ground in a high-shear cutting mill, sieved to a size fraction of 106–150 μm and then dried in small batches in an air-circulating oven at 308 K for 16 h to remove free moisture. Ultimate and proximate analyses of the different biomass varieties investigated in this study are provided in Table 1.

The limestone (Purbeck, UK) and dolomite (Steetley Dolomite Ltd) samples were prepared by grinding in a hammer mill followed by sieving to a size fraction of 355–425 μm. XRF analyses of the silica sand (David Ball Sand, 500–710 μm), dolomite and limestone are presented in Table 2. Different size fractions of sand and catalyst were used to enable facile separation of the materials retrieved from the beds after experiments for analysis.

Table 1
Proximate and ultimate analyses of the biomass samples used in this study.

Feed	Ultimate Analysis [daf]						Proximate Analysis		
	C	H[a]	N	O[b]	S	Cl	Ash	Moisture	Volatiles
Beech wood (BW)	49.3	5.5	0.3	44.9	< 0.04	0.01	0.5	11.6	75
Brazilian rice husk (BRH)	43.1	5.6	0.4	50.9	< 0.04	0.02	13.4	6.9	45.2
Thai rice husk (TRH)	47.0	5.9	0.8	46.0	0.05	0.40	16.8	10.1	64.5
Textile Industry Residue (TIR)	57.5	9.0	4.9	22.3	3.99	1.65	29.0	11.9	53.0

Values for the proximate analyses are calculated on the "as received" moisture.
[daf] dry, ash-free basis.
The analysis for beech wood and Thai rice husk was carried out by TES Bretby, UK.
The analysis for the Brazilian rice husk and textile sludge residue was carried out by H.Jorge, Private Comm, 2010.
[a] Denotes that the value has been corrected for moisture content *i.e.* it does not include the hydrogen in the moisture.
[b] The oxygen content was determined by difference.

Table 2
XRF Analysis of the Sand, Dolomite and Purbeck Limestone used in this study.

Constituent	Sand [wt.%]	Limestone [wt.%]	Dolomite [wt.%]
CaO	0.20	93.15	65.25
SiO_2	98.41	8.46	0.14
MgO	0.00	0.76	34.47
Fe_2O_3	0.10	0.55	0.04
Al_2O_3	1.09	0.47	0.08
P_2O_5	0.00	0.22	0.00
SO_3	0.00	0.15	0.00
K_2O	0.17	0.11	0.00
SrO	0.00	0.07	0.02
MnO	0.00	0.05	0.00
NiO	0.00	0.01	0.00
TiO_2	0.03	0.00	0.00

Table 3
Summary of experimental operating parameters.

Operating Conditions	1st Stage	2nd stage
Fuel type	Beech wood Thai Rice Husk Brazilian Rice Husk Textile Industry Residue	–
Fuel weight	1.000 g	–
Fuel Particle Size	106–150 μm	–
Bed type	–	Variable: No bed 20 mm Sand (500–710 μm) 20 mm Sand & Dolomite (10–40 wt%)[a] 20 mm Sand & Limestone (20 wt %)[a]
Heating Rate	1 K s^{-1}	Preheated to experimental temperature
Hold Temperature	773 K	Variable- 973 K 1073 K 1173 K
Hold Time	900 s	–
Pressure	2.2 bar_a	2.0 bar_a
Carrier Gas	Helium	Helium
Superficial Velocity	0.1 m s^{-1}	0.25 m s^{-1}

[a] Limestone and dolomite 355–425 μm.

2.2. Operating conditions

A standard set of conditions (summarised in Table 3) was used when operating the reactor in either its single or 2-stage configuration. Biomass samples loaded into the 1st stage were heated at a rate of 1 Ks^{-1} from ambient to 773 K where the reactor was held for 900 s to ensure complete pyrolysis of the sample. An inert flow of helium with superficial velocity of 0.1 m s^{-1} at 773 K was introduced at the top of the reactor to sweep evolving volatiles from the sample bed downstream to the 2nd stage or tar trap.

The operating conditions of the 2nd stage were varied depending on the variable that was being tested. In all cases, the 2nd stage was heated to the experimental temperature (973–1173 K) prior to starting the first stage temperature program. Beds containing limestone and dolomite were preheated to 1173 K for 300 s to ensure the dolomite and limestone was fully calcined before cooling to the experimental temperature. The tar trap was not cooled during the preheating period to avoid trapping any of the CO_2 or H_2O released as a result of moisture loss and/or calcination of the 2nd stage bed materials. An additional flow of He was added through gas inlets in the 2nd stage flange so that a constant superficial flow of 0.25 m s^{-1} was maintained through the 2nd stage for all the investigated temperatures.

2.3. Product recovery

After each experiment, the reactor was dismantled, the beds were removed and the reactor components washed with a 4:1 (v/v) solution of chloroform and methanol (150 ml) to recover the tar. The washings were filtered into a flask using a pre-weighed Whatman no. 1 filter paper to collect any chars that were removed in the washing process. The bulk of the solvent was removed on a rotary evaporator (BUCHI-Rotavapor 3000) operated at 353 K and 40 rpm for 10 min. The tar was then transferred to an aluminium beaker and placed in a recirculating air oven at 308 K for 2 h (along with the chars that were removed from the 1st stage after the washing step) to ensure complete solvent removal from the samples. The recovered tar and char samples were then weighed to determine their respective gravimetric yields. All tar and char yields are presented on a dry, ash-free basis.

The concentration of CO (Servomax Xentra 420, 0–25 vol%) and CH_4 (ADC, 0–20 vol%) were measured in the reactor effluent after the tar trap via online gas detectors. CO_2 was also measured by online gas detection (Servomax xentra 4200, 0–100 vol%) but condensed in the tar trap during the experiments and so was measured after the experiments were completed as the tar trap warmed up to room temperature.

Experiments were repeated at least three times. All graphically presented data points are provided with an associated error range of a single standard deviation on either side of the mean unless otherwise stated.

2.4. Product characterisation

Size exclusion chromatography (SEC) was used to determine the molecular size distribution of the tar samples. The SEC setup consisted of a Mixed D column (300 mm long, 7.5 mm id) with a poly-divinylbenzene packing (5 μm particle size) supplied by Polymer Laboratories UK. Tar samples were dissolved in n-methyl pyrrolidone (NMP) which was used as the mobile phase. A full description of the SEC setup and operating procedure used in this work has been presented elsewhere [45].

Ultra-violet fluorescence (UV-F) analysis (Perkin-Elmer LS50 luminescence spectrometer) of the tar samples was performed to provide information on the degree of conjugation and to an extent, the size of tar components. Tar samples were dissolved in NMP and irradiated with UV light (254–800 nm, 0.5 nm step size). Excitation and emission wavelengths were changed simultaneously with a fixed 20 nm difference in wavelength corresponding to Stokes shift. Both the wavelengths of light that a sample component absorbs and subsequently fluoresces increase with degree of conjugation.

Elemental analysis of the tar and char samples to determine the concentration of carbon, hydrogen, nitrogen, sulfur and oxygen (by difference) was carried out using a Perkin Elmer 2400 at the University of Sheffield. Trace elements analysis of the chars was carried out via neutron activation analysis (NAA) at the Centre for Analytical Research in the Environment, Silwood Park, Ascot [46].

Pore surface area (BET) and pore volume distribution (BJH) measurements of the recovered chars and bed materials were determined by N_2 adsorption measurements (Micromeritics Tristar 3000 N_2 sorption analyser). Pore volume distribution in the macroporous range was carried out via mercury porosimetry (Micromeritics IV 9500 series analyser). Sample morphology was observed by scanning electron microscopy (SEM) (Hitachi S3400) with 20 kV of accelerating voltage under high vacuum. The samples were coated with gold before SEM examination. Images obtained by secondary electrons are presented here.

Char reactivity measurements with air and CO_2 were carried out using a TGA (TA Q5000). Between 3 and 5 mg of char sample was loaded onto a platinum pan and heated under a flow of N_2 (25 ml min^{-1}) to either 773 K or 1173 K for reactivity measurements with air and CO_2 respectively. The temperature was held at the set-point temperature for 300 s before the gas purge was switched to either air or CO_2. The weight loss of the chars was observed until constant weight was obtained. The normalised maximum reactivity (R_{max}) was obtained from the maximum rate of reaction (maximum rate of weight loss) using equation (1).

$$R_{max} = -\frac{1}{Wo}\left(\frac{dW}{dt}\right) \tag{1}$$

Where W_0 is the initial weight of the char (daf basis), and (dW/dt) is the rate of weight loss, obtained from the first derivation of the weight loss curve. The repeatability of the R_{max} determination is ± 9% of the value quoted. Only single determinations have been reported as the repeatability is usually high and well within ± 5% of the measured reactivity value.

The extent of coking of the bed materials recovered from the reactor was also examined using TGA analysis. Samples were heated under a flow of N_2 (25 ml min^{-1}) in stages up to 1123 K. The first stage involved heating the sample to 383 K to remove free moisture, the sample was then heated to 683 K to calcine any magnesium carbonate and chemically bound moisture in the form of a hydrate that may have formed. Calcination of calcium carbonate took place as the temperature was increased further to 1123 K. The flow of N_2 was then switched to air to combust coke deposits on the surface of the materials.

3. Results and discussion

3.1. Single-stage pyrolysis results

3.1.1. The influence of biomass feedstock on the primary pyrolysis product distribution

The product distributions for the pyrolysis of the different biomass feedstocks (Fig. 2) demonstrated similar trends to those observed in the proximate analysis (Table 1). Beech wood (BW) produced the largest amount of volatiles (liquids and gases) whilst the textile industry residue (TIR) exhibited the reverse trend producing the largest amount of char and least volatiles. Pyrolysis of the two rice husk species produced similar amounts of char and volatiles to the beech wood, although the Thai rice husk (TRH) produced approximately 40% less tars than the Brazilian rice husk (BRH). BW pyrolysis yielded a similar amount of tar

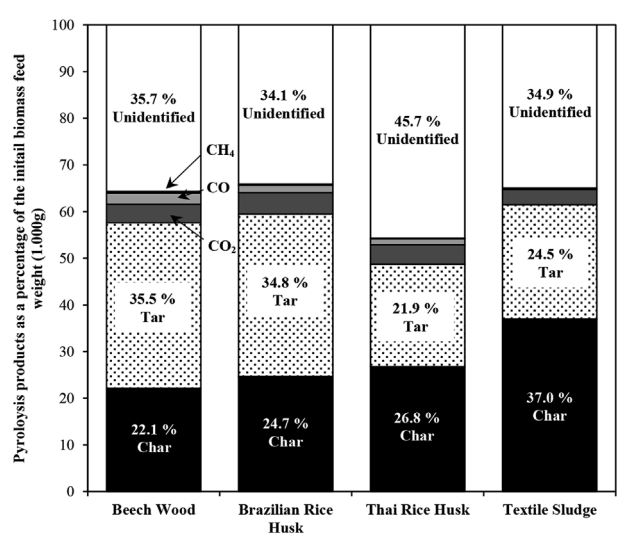

Fig. 2. Distribution of the products generated during pyrolysis of four types of biomass feed in the single stage reactor presented on a dry, ash-free basis. All errors were less than 0.5% of the mean. **Gas Yields**: CO_2 = 3.9% 4.6% 4.2%, 3.3%; CO = 2.4%, 1.6%, 1.3%, 0.2%; CH_4 = 0.3%, 0.2%, 0.1%, 0.2% for BW, BRH, TRH and TS respectively. **Experimental Parameters**: ***1st stage***: **Feed** = Variable (1.000 g, 106–150 μm), **carrier gas** = He, **superficial velocity** = 0.1 m s^{-1}, **inlet pressure** = 2.2 bar_a, **heating rate** = 1 K s^{-1}, **hold temperature** = 773 K, **hold time** = 900 s.

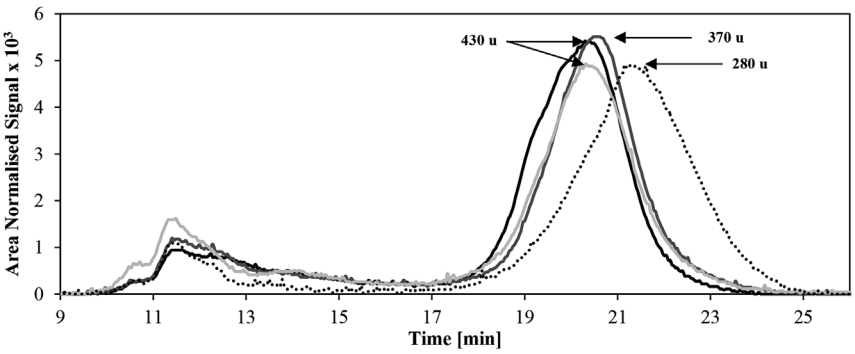

Fig. 3. SEC analyses of the tars recovered after pyrolysis of the four types of biomass feed in the single stage reactor. **Experimental Parameters**: ***1st stage***: **Feed** = Variable (1.000 g, 106–150 μm), **carrier gas** = He, **superficial velocity** = 0.1 m s^{-1}, **inlet pressure** = 2.2 bar_a, **heating rate** = 1 K s^{-1}, **hold temperature** = 773 K, **hold time** = 900 s.
BW; BRH; TRH; TIR.

to the BRH at 35.5 wt%. The tar yield in the case of the TIR pyrolysis was lower at 24 wt% than the BW and BRH pyrolysis but higher than the tar yield of the TRH pyrolysis at 21.9 wt%

The amount of char produced during pyrolysis increased with increasing ash content as determined by proximate analysis (Table 1). This is consistent with previous works that have concluded a high ash content favours char-forming reactions [47,48]. Yields of the measured combustible gases (CO and CH_4) were relatively low in all cases ranging from 0.3 wt% for TIR to 2.7 wt% for beech wood. CO_2 yields were slightly higher in the region of 3–5 wt%.

Between 35 and 45 wt% of the pyrolysis products could not be accounted for. The unidentified products were likely to have included compounds such as light tar species, light hydrocarbons, alcohols, water and hydrogen that were either not efficiently trapped during the experiment or lost during the product recovery procedure. Previous biomass pyrolysis investigations with the 2-stage reactor reported water yields of between 15 and 27 wt% of the total mass balance depending on the temperature and gas superficial velocity in the empty 2nd reactor stage [43,44].

A comparison of the results presented in this paper with similar pyrolysis studies reported in the literature referencing beech wood and rice husk reveals reasonably high variability. Dabai et al. reported a very similar product distribution for the pyrolysis of beech wood to those reported here, albeit using the exact same reactor, beech wood feedstock and very similar conditions [44]. Nik-Azar et al. also reported similar tar and char yields of 30–35 wt% and 20 wt% respectively for the pyrolysis of an untreated beech wood in a wire mesh reactor when heated to 773 K (heating rates reported as $\leq$ 100 Ks^{-1}) [49]. Faster heating rates of 1000 Ks^{-1} (peak temperature ~ 1373 K) were found to produce higher tar yields of up to 50–55 wt% and lower char yields of ~15 wt%. Westerhoff et al. reported much higher oil yields of between 60 and 65 wt% and lower char yields of 8–12 wt% for the fast pyrolysis of milled beech wood pellets (similar particle sizes to those used here) in a fluidised bed reactor at 773 K [50].

Somrang et al. investigated the pyrolysis behaviour of the exact same beech wood and Thai rice husk samples in a wire mesh reactor [51]. The char yield produced from the pyrolysis of the Thai rice husk in the wire mesh reactor heated at 1 K s^{-1} to 773 K was slightly lower at 21 wt% compared with 26.8 wt% produced from the fixed bed used here. However, the tar yield was substantially larger, at around 39 wt%. A higher tar yield and lower char yield was to be expected in the case of the wire mesh reactor where the residence time within the reactor and char bed is significantly lower than in the case of the fixed bed reactor (i.e. less time for char forming/tar cracking reactions to take place) [33]. It should also be noted that we report the tar yield on a dry, ash-free basis whereas Somrang et al. reports the bio-oil yield on an ash-free basis (*i.e.* including water) which further contributes to the large discrepancy in tar/oil yields.

Tsai et al. reports tar and char yields of 39 wt% and 33–34 wt% respectively for the pyrolysis of a Taiwanese rice husk (< 500 mm, 11–21 g inventory) in a fixed bed reactor heated to 773 K at 200 $Kmin^{-1}$ (hold time of 8 min) [52]. Qian et al. reported char yields of ~34 wt% and oil yields of 27–36 wt% (depending on whether a fixed superficial or volumetric flow rate was applied) for the pyrolysis of a Chinese rice husk (0.15–0.45 mm, 4 g inventory) in a fixed bed reactor heated to 973 K at 15 K min^{-1} [53]. The char yields increased slightly to 39 wt% whereas the oil yields decrease to ~15 wt% when the pressure was increased to 6 bar_a.

At this point it is important to stress that comparisons of the pyrolysis product distributions presented here and those from similar studies reported in the literature is complicated. As this paper demonstrates, biomass of the same variety (rice husk in the case of this paper) can display dramatically different pyrolysis product distributions due to differences in the location from which they were sourced (*i.e.* differences in soils, climate, harvesting/processing protocols, strain *etc.*). The type of reactor, temperature, pressure, particle size, pre-treatment protocols, moisture content, product recovery protocols *etc.* also make comparisons between different studies difficult. The intention of the first part of this paper was to use simple, high throughput pyrolysis experiments to investigate the thermochemical breakdown behaviour of different biomass feedstocks and determine the influence of inherent biomass properties on the distribution and characteristics of the pyrolysis products (see section 3.2 for a more detailed discussion). Ultimately this type of study could be applied to provide a preliminary assessment of the suitability of different biomass feedstocks for use in biomass gasification applications. Further, more rigorous testing of promising biomass feedstocks in systems that better approximate a biomass gasifier would be necessary to fully establish the gasification behaviour and determine the optimal gasifier design and operating conditions.

3.1.2. Tar analysis

Each of the SEC chromatograms had two peaks separated by a region of low absorption intensity revealing that the tar samples had a bimodal molecular size distribution (Fig. 3). The first (excluded) peaks correspond to the elution of high molecular mass tar constituents that were excluded from the porosity of the column.

The second (retained) peaks in the SEC chromatograms correspond to the elution of lower molecular mass tar constituents which were retained and could therefore be fully resolved by the column. The molecular mass corresponding to the maximum peak intensities were estimated and are provided in Fig. 3.

The most notable difference in the SEC chromatograms is in the elution time of the lighter fraction (retained peak) of the TIR tars. The maximum intensity appeared almost 1 minute after the equivalent peaks in the chromatograms of the other tar samples indicating that the lighter fraction of the TIR tar had a lower average molecular mass compared with the tar produced from pyrolysis of the more conventional biomass varieties.

There were also differences in the SEC chromatograms of the pyrolysis tar of the two rice husk species. The TRH tar had a slightly larger proportion of the heavier tar fraction relative to the lighter fraction

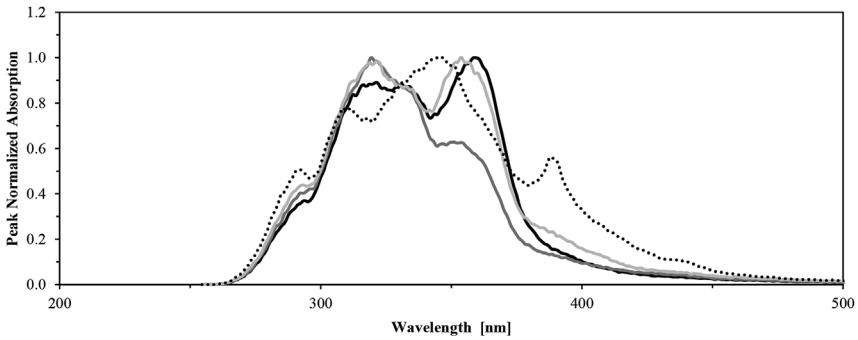

Fig. 4. UVF analyses of the tars recovered after pyrolysis of the four types of biomass feed in the single stage reactor. **Experimental Parameters**: ***1st stage***: **Feed** = Variable (1.000 g, 106–150 μm), **carrier gas** = He, **superficial velocity** = 0.1 m s^{-1}, **inlet pressure** = 2.2 bar_a, **heating rate** = 1 K s^{-1}, **hold temperature** = 773 K, **hold time** = 900 s.
BW; BRH; TRH; TIR.

compared with the Brazilian variant. The maximum peak intensity of the retained peak in the chromatogram of the TRH tar also appeared at a slightly shorter elution time than the equivalent peak in the chromatogram of BRH tar indicating that the lighter fraction of the TRH tar had a higher average molecular mass of 430 u compared with 370 u in the case of the BRH tar.

The UVF spectra of the three biomass tar samples consisted of a broad emission spectrum between ~270 and 450 nm with two maxima at ~320 nm and ~350–360 nm (the small peaks in each of the spectra at ~290 nm was caused by fluorescence emissions from the solvent-NMP). The presence of the two, relatively well defined peaks indicates that the lighter tar fraction of the biomass tar (as characterised by SEC) broadly consisted of two molecular groups that differed by extent of conjugation. (UVF is only able to detect compounds with molecular masses < 3000 u and so does not provide any information on the tar species characterised by the excluded peaks in SEC spectrums.)

There were notable differences between the UVF spectra of the tars derived from the two rice husk species (Fig. 4). The first peak in the spectra of the BRH tar at ~320 nm was far more intense than the second peak at the higher wavelength of ~355 nm whereas the two peaks in the spectra of the tar derived from the Thai variant were of equal intensity. These observations indicate that there was a larger proportion of the less conjugated tar species in the BRH tars relative to the more conjugated tar species; whereas the tar derived from the Thai variant contained similar quantities of the two conjugated molecular groups.

The spectra of the pyrolysis tar derived from the TIR was distinctly different from the spectra of the three biomass derived tars- it was broader and consisted of a large central peak at around 340 nm flanked by two less intense peaks at 310 nm and 390 nm.

Elemental analysis of the different pyrolysis tars (Table 4) revealed that in all cases, the tars had slightly higher carbon contents and slightly lower oxygen contents than their parent biomass. The compositional trends in the carbon and oxygen contents of the different pyrolysis tars were the same as those observed for the different parent biomass feedstocks. The BW and BRH tars had similar carbon and oxygen contents of around 55 wt% and 40 wt% respectively whereas the TRH and TIR tars had slightly higher carbon contents of around 60 wt% and lower oxygen contents of 33 wt% and 22 wt% respectively. The higher carbon content and significantly lower yield of the TRH tar relative to the BRH tar is indicative of a greater extent of tar cracking in the case of the TRH tars [54].

3.1.3. Char analysis

Trends in the elemental analysis of the chars were different to those observed for the tars (Table 5). The BW char had the highest carbon content and lowest oxygen content at 80.3 wt% and 16.6 wt% respectively. The carbon contents of the rice husk derived chars were slightly lower at 72–75 wt%. The TIR char had the lowest carbon content and highest oxygen content at 61.9 wt% and 28.7 wt% respectively. Interestingly, the carbon content of the TIR char was similar to that of the tar but contained a larger proportion of oxygen compared with its respective tar which contained more hydrogen and nitrogen.

In addition to ultimate analysis, the concentrations of certain trace elements in the chars were determined via nuclear activation analysis (NAA) (Fig. 5). Determining the concentration of the alkali and alkaline earth metals such as K, Na, Ca and Mg is particularly important given their known catalytic activity during pyrolysis, char gasification and tar cracking interactions [55–59]. The TIR char was found to contain the largest concentrations of sodium, calcium and magnesium, however the TRH char contained the largest amount of potassium. The TRH char also contained more of all the alkaline and alkaline earth metals measured in this study (Na, K, Ca and Mg) than the BRH char, which in the case of potassium was over double the amount detected in the BRH char. The BW char also contained reasonably high concentrations of the alkali and alkaline earth metals particularly Ca of which it contained around 3–4 times more than the rice husk chars. The BW char contained less magnesium than the other chars but a similar amount of potassium to the BRH and TIR chars.

Surface area and pore size distribution analysis of the char particles

Table 4
Summary of the elemental analysis results for the tars produced from the pyrolysis of the different biomass feedstocks in the single stage reactor.
Experimental Parameters: ***1st stage***: **Feed** = Variable (1.000 g, 106–150 μm), **carrier gas** = He, **superficial velocity** = 0.1 m s^{-1}, **inlet pressure** = 2.2 bar_a, **heating rate** = 1 K s^{-1}, **hold temperature** = 773 K, **hold time** = 900 s.

Tars	Ultimate Analysis (wt.%) [daf]				Atomic Ratio		
	C	H	N	O[a]	O/C	H/C	N/C
Beech wood (BW)	55.4	6.4	0.1	38.1	0.5	1.4	0.00
Brazilian rice husk (BRH)	53.1	5.9	0.9	40.0	0.6	1.3	0.01
Thai rice husk (TRH)	59.0	6.7	1.3	33.0	0.4	1.4	0.02
Textile industry residue (TIR)	61.5	8.7	8.1	21.8	0.3	1.7	0.11

[a] The oxygen content was determined by difference.

Table 5
Summary of the elemental analysis results for the tars produced from the pyrolysis of the different biomass feedstocks in the single stage reactor. **Experimental Parameters**: ***1st stage***: **Feed** = Variable (1.000 g, 106–150 μm), **carrier gas** = He, **superficial velocity** = 0.1 m s^{-1}, **inlet pressure** = 2.2 bar_a, **heating rate** = 1 K s^{-1}, **hold temperature** = 773 K, **hold time** = 900 s.

Char	Ultimate Analysis (wt.%) [daf]				Atomic Ratio		
	C	H	N	O[a]	O/C	H/C	N/C
Beech wood (BW)	80.3	2.7	0.3	16.6	0.2	0.4	0.0
Brazilian rice husk (BRH)	74.6	3.1	1.4	20.9	0.2	0.5	0.0
Thai rice husk (TRH)	72.3	3.0	1.0	23.7	0.2	0.5	0.0
Textile industry residue (TIR)	61.9	5.1	4.3	28.7	0.3	1.0	0.1

[a] The oxygen content was determined by difference.

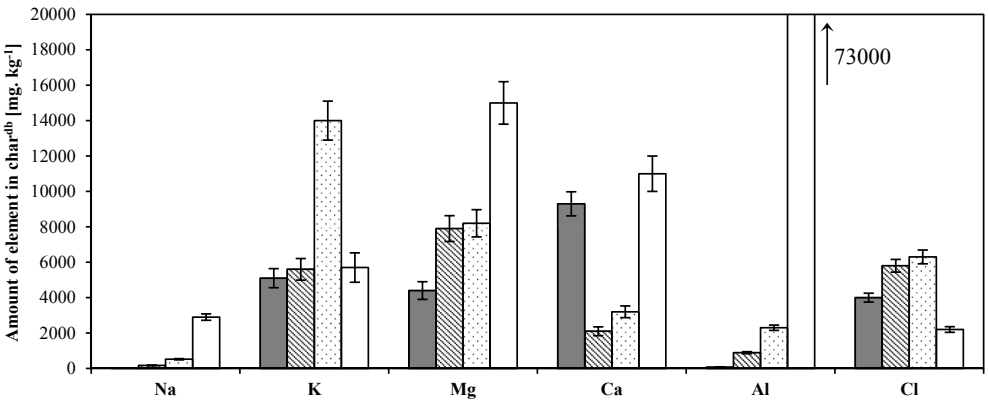

Fig. 5. The amounts of certain important inorganic elements present in the chars produced during pyrolysis of the different biomass feedstocks in the single-stage hot-rod reactor determined via nuclear activation analysis. **Experimental parameters**. ***1st stage***: **Feed** = Variable (1.000 g, 106–150 μm), **carrier gas** = He, **superficial velocity** = 0.1 m s^{-1}, **inlet pressure** = 2.2 bar_a, **heating rate** = 1 K s^{-1}, **hold temperature** = 773 K, **hold time** = 900 s.
■BW; ▨ BRH; ⬚ TRH and □ TIR.

Table 6
Summary of BET/BJH N_2-adsorption and Hg-porosimetry results for the chars obtained after pyrolysis of the different biomass feedstocks in the single-stage, hot-rod reactor. **Experimental Parameters**: ***1st stage***: **Feed** = Variable (1.000 g, 106–150 μm), **carrier gas** = He, **superficial velocity** = 0.1 m s^{-1}, **inlet pressure** = 2.2 bar_a, **heating rate** = 1 K s^{-1}, **hold temperature** = 773 K, **hold time** = 900 s.

Char	BW	BRH	TRH	TIR
Surface Area [m^2g^{-1}]	1.2	12.3	6.9	41.3
Average mesopore diameter, d_{mesp} (2–50 nm) [nm][a]	9	5	7	10
Average macropore diameter, d_{macp} (50–10^5 nm) [nm][a]	1490	130	250	10
Cumulative vol. of mesopores (2–50 nm) [cm^2 g^{-1}]	6.3×10^{-3}	2.7×10^{-2}	1.7×10^{-2}	0.106
Cumulative vol. of macropores (50–10^5 nm) [cm^2 g^{-1}]	0.433	0.401	0.427	6.8×10^{-2}

Where V_p is the volume of pores determined via BJH for mesopores or MIP for macropores and A is the BET surface area.
[a] Average pore diameters were calculated using the Gurwitch rule i.e. d_{mesp} (or d_{macp}) = $4V_p/A$

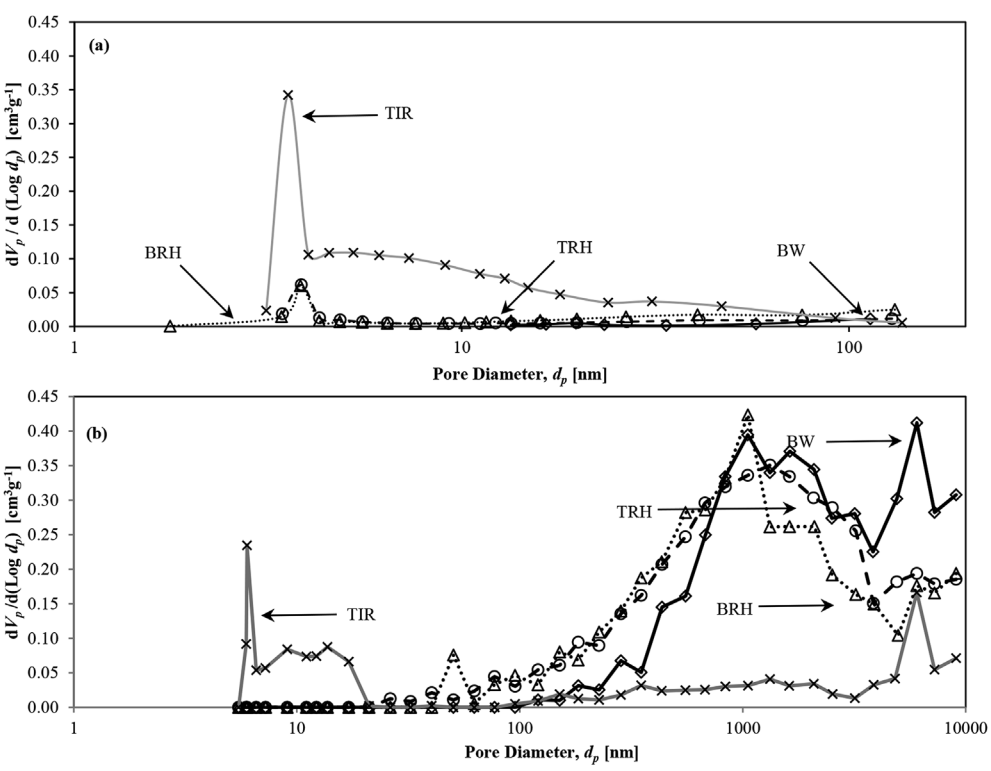

Fig. 6. Pore size distributions for (a) the pore size range 1.7–300 nm as determined via BJH N_2 adsorption analysis and (b) the pore size range 5–10000 nm as determined via mercury porosimetry for the chars obtained after pyrolysis of the different biomass feedstocks in the single-stage, hot-rod reactor. **Experimental Parameters**: ***1st stage***: **Feed** = Variable (1.000 g, 106–150 μm), **carrier gas** = He, **superficial velocity** = 0.1 m s^{-1}, **inlet pressure** = 2.2 bar_a, **heating rate** = 1 K s^{-1}, **hold temperature** = 773 K, **hold time** = 900 s. —◇— BW; ····△···· BRH; — ⊖ — TRH and —×— TIR.

via BET/BJH N_2-adsorption analysis revealed that the TIR char had the highest surface area at 41 m^2 g^{-1} (Table 6) and largest concentration of pores in the meso-porous region (2–50 nm) (Fig. 6a). The cumulative volume of pores of the TIR char as measured by BJH analysis was almost two orders of magnitude larger than the chars produced from the other biomass feedstocks at 0.11 cm^3 g^{-1}. The BW char had the smallest surface area and least volume of mesopores. There were also some differences between the two rice husk species with the BRH char exhibiting almost double the surface area and volume of mesopores compared with the TRH char.

Analysis of the macroporosity via mercury porosimetry revealed that the TIR char had the least macro-porosity at 0.07 cm^3 g^{-1} compared with ~0.40–0.43 cm^3 g^{-1} for the other chars (Fig. 6b, Table 6). The average pore size in the macroporous region (50–10^5 nm) varied

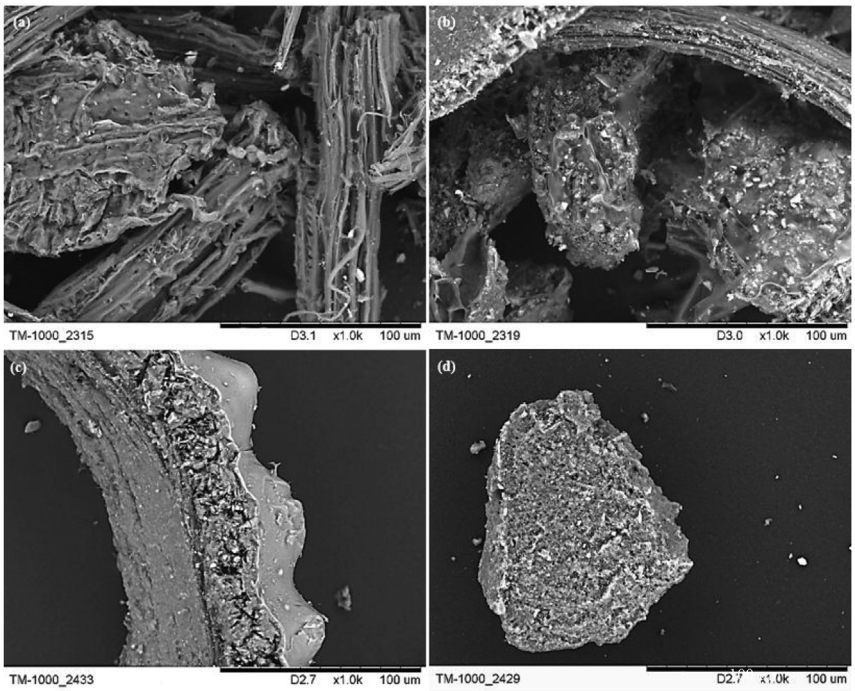

Fig. 7. SEM images of the chars produced during the pyrolysis of the different feeds in the single stage reactor. (a) BW chars, (b) BRH chars, (c) TRH char, (d) TIR char. **Experimental Parameters**: ***1st stage***: **Feed** = Variable (1.000 g, 106–150 μm), **carrier gas** = He, **superficial velocity** = 0.1 m s^{-1}, **inlet pressure** = 2.2 bar_a, **heating rate** = 1 K s^{-1}, **hold temperature** = 773 K, **hold time** = 900 s.

substantially. The BW char was found to have the largest average pore size at 1490 nm. The average pore sizes of the rice husks were an order of magnitude smaller than the BW at 130 nm and 250 nm for the BRH and TRH chars respectively. The TIR char had the smallest average pore size which was an order of magnitude smaller again at 10 nm. A trend can be observed between the initial ash content of the parent biomass and the surface area, volume of mesopores and average pore size in both the meso- and macro-porosity regions of the char with the higher ash content appearing to favour smaller pores and a higher surface area.

A comparison of the surface structures and morphologies of the different char particles via SEM analysis revealed that the BW char particles had the most fibrous structure and largest pores whilst the TIR chars have the smallest pores (Fig. 7a,d). The two rice husk chars appeared to have slightly smaller pores (Fig. 7b and c) than the BW char. These observations were consistent with the trends in macroporosity determined via mercury-porosimetry. The surface of the rice husk and TIR chars also appeared to be coated with a lot more ash (lighter-coloured areas in Fig. 7a–d) compared with the BW char particles which in the case of the rice husk chars appeared to have formed some sort of molten phase.

Thermogravimetric analysis of the chars was used to determine their relative reactivities in air at 773 K and CO_2 at 1173 K. The BW and TRH chars exhibited the highest peak reactivities in air at 773 K exhibiting a maximum normalised reactivity of 0.012 g $g^{-1}s^{-1}$; and observed similar reactivity profiles (Fig. 8). In both cases, the combustion reaction rate increases reaching maxima at conversion values of 0.37 and 0.12 for the BW char and TRH char respectively.

The peak normalised reactivities of the BRH and the TIR chars were lower than those observed for the BW and TRH chars at 0.007 g $g^{-1}s^{-1}$. These chars also exhibited similar combustion reactivity profiles (albeit different profiles to the BW and TIR chars) reaching maximum reactivities at conversions of < 0.02 followed by a steady monotonous decline with increasing conversion.

The reactivity profiles of the chars reacting with CO_2 at 1173 K were quite different to those observed for the air reactivity experiments at 773 K (Fig. 9). In the case of the BW and rice husk chars, the reactivity profiles show an initial surge in reactivity coinciding with the entry of the reactive gas, a reactivity which rapidly declines to a much lower stable value. The BW char transitioned to the post surge stable

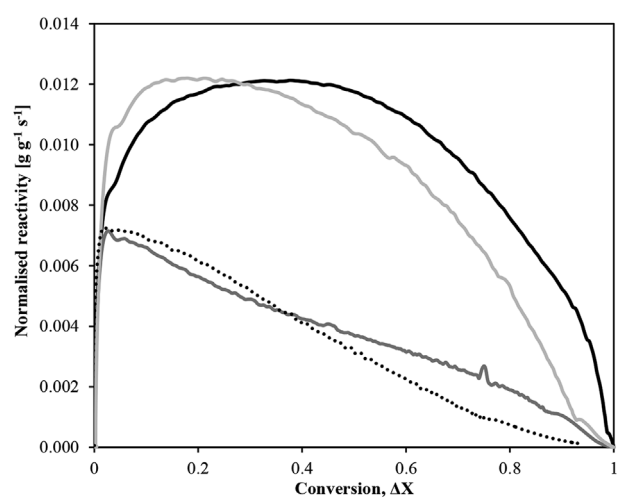

Fig. 8. Normalised combustion reactivities of the four different chars with air at 773 K as a function of conversion.
BW; BRH; TRH; TIR.

reactivity at a conversion of 0.27 and achieved complete char gasification conversion within 10 min. The BRH and TRH char gasification transitioned at a much lower conversion of around 0.05 and due to the much slower post-surge gasification reactivities required much longer time periods of 140 min and 70 min for the BRH and TRH respectively to achieve complete conversion. The reactivity profile for the TIR char was different to those observed by the other chars in that the initial surge persisted for close to the entire conversion range, transitioning to the post-surge reactivity behaviour at a conversion of ~0.89 achieving complete conversion after ~2 min.

As indicated above, the TIR char exhibited the highest initial peak reactivity of 0.060 g $g^{-1}s^{-1}$ with the BW char displaying the second highest reactivity of 0.024 g $g^{-1}s^{-1}$. The BRH and TRH chars were significantly less reactive with peak normalised reactivities of 0.005 g $g^{-1}s^{-1}$. The stable residual reactivities measured at a conversion of 0.5 (or 0.9 for the TIR char) were between 14 and 17 times lower than the maximum reactivities measured during the initial surge

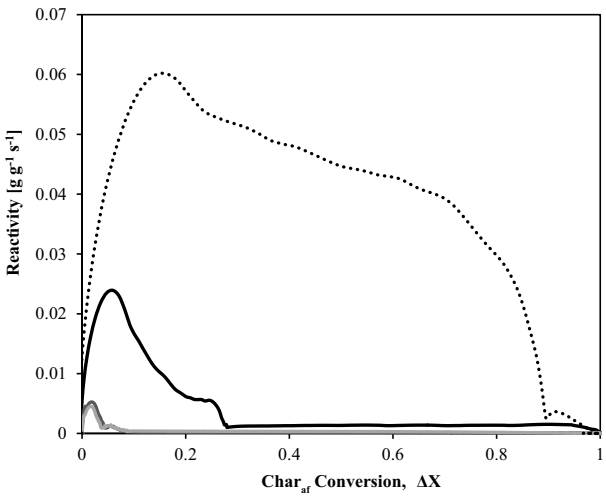

Fig. 9. Normalised CO_2 gasification reactivities of the four different chars at 1123 K as a function of conversion.
BW; BRH; TRH; TIR.

for the BW, TRH and TIR chars and 35 times lower in the case of the BRH char. The trend in residual char gasification reactivities with CO_2 at 1173 K was: TIR char > BW char > TRH char > BRH char.

3.2. Discussion of single stage primary pyrolysis results

Pyrolytic decomposition of biomass and other carbonaceous materials is a complex process involving a multitude of different reactions. The resultant distribution and nature of the pyrolysis products depends on a range of different process parameters and fuel properties. In this work, the four different biomass varieties were prepared and tested in the same way such that any differences in the observed pyrolysis product distributions were a result of inherent differences in the properties of the parent biomass feeds. The O/C ratio of the parent biomass, lignocellulosic composition, ash content and phase composition, pore structure and surface area development during pyrolysis have all been reported to affect the pyrolysis behaviour of a particular biomass fuel [44,47,48,60–63].

The most striking differences in the pyrolysis product distributions is between the two rice husks species with the Brazilian variant releasing ~40 wt% more tar than the Thai rice husk. Whilst there were small differences in the elemental compositions of the parent biomasses as well as small differences in the surface areas and morphologies of the resultant chars; the most likely cause for the differences in the tar and gas yields between the TRH and BRH pyrolysis experiments was the difference in potassium concentration. The potassium concentration of the TRH was more than double the concentration of the other biomass varieties all of which contained similar quantities.

Pyrolysis of biomass varieties containing large amounts of ash are typically found to produce less tar and more char due to the catalytic effect and higher surface area provided by the inorganic ash constituents on which secondary tar condensation/char forming reactions can take place [63,64]. An exception to this rule is when the ash contains high concentrations of potassium, which has been found to act as a strong gasification catalyst during pyrolysis promoting reactions between the evolving tars with other primary pyrolysis products such as CO_2 and H_2O [55,65]. These interactions have the effect of reducing liquid formation (and in some cases char formation) in favour of gas formation as was observed here [55]. Similar results were reported by Morgan et al. who found that bio-oil yields from the fast pyrolysis of semi tropical biomass in a fluidised bed were improved when the biomass was pre-treated or washed in cold water to remove some of the easily removable alkali and alkaline earth metal salts in the sample [66,67]. Nik-Azar et al. also reported lower tar yields and higher gas yields from the pyrolysis of beechwood impregnated with pottassium [49]. In both cases, char yields appeared to be insensitive to the pretreatment procedure demonstrating similar pyrolysis behaviour to the rice husk species studied here where the mineral content variation was natural.

The SEC results show that the TRH tars contained a larger proportion of the heavier tar fraction (characterised by the excluded peak in the SEC chromatogram) compared with the BRH tars. The peak corresponding to the lighter tar fraction also eluted at a shorter time which was most likely due to the larger proportion of a more conjugated group of tar compounds present in the TRH tars as indicated by UVF analysis. These findings suggest that the enhanced tar cracking afforded by the higher concentration of potassium in the TRH, favoured the cracking/gasification of the lighter, less conjugated tar fractions.

The pyrolysis behaviour of the TIR adhered far better with the trend typically observed for biomass containing large quantities of ash in that it produced more char and less tar whilst the amount of gas/unidentified products yield was similar to the BW and BRH.

The nature of the TIR tar (as characterised by SEC and UVF) was quite different to the tars derived from the other biomass feeds tested in this study. SEC indicated that the TIR tar contained a larger proportion of the lighter tar fraction (resolved peak in the SEC chromatogram) which also had a lower average molecular mass than the other tar samples. The UVF spectra of the pyrolysis tar derived from the TIR was also different-the spectra was broader and was comprised of three peaks compared to two.

One possible cause of the differences in the nature of the TIR tars can be deduced from the morphology of the resultant char. The N_2-adsorption and Hg-porosimetry analysis revealed that the TIR char had the highest surface area and a predominantly mesoporous pore structure compared with the other biomass derived chars which were largely macroporous in nature. These combined properties infer that the residence time of the volatiles within the char matrix and contact between the volatiles and the char pore wall would have been greater than for the other biomass varieties. A greater residence time of the volatiles in the char in addition to the high concentration of inorganic matter would have caused enhanced secondary tar polymerisation and char forming reactions. This is particularly true for the larger primary tar compounds which are likely to have been hindered from exiting the char by the small pores resulting in the evolution of smaller, lower molecular weight tar compounds.

It should also be noted that the differences observed in the product distribution and nature of the tars and char could be due to compositional differences (compared with the more conventional lignocellulosic biomass varieties tested here) and related differences in the thermo-chemical breakdown pathways. Unfortunately, it is not possible to expand further on the potential differences in the thermo-chemical breakdown pathways without more in depth compositional information of the different feeds which was not available at the time of this study.

The product distributions of BW and BRH pyrolysis and nature of the tars as determined by SEC and UVF analysis were very similar despite the differences in the O/C ratios, ash content (particularly the inert ash component content), surface area and porosity of the resultant char. This indicates that these factors have less influence on the pyrolysis behaviour compared with the concentration of certain catalytically active ash constituents.

Determining the reactivity of the pyrolysis char is particularly important when designing a gasification process for a particular fuel. The BW and TRH chars demonstrated the highest normalised reactivities in the combustion tests of 0.012 g $g^{-1}s^{-1}$ while the reactivities of the BRH and TIR were lower at 0.007 g $g^{-1}s^{-1}$. There were also similarities in the reactivity profiles as a function of conversion between the more reactive BW and TRH chars and the less reactive BRH and TIR chars (Fig. 8). The combustion reactivity profile of the BW and TRH chars initially increased, passing through a maximum reactivity at

intermediate conversions of 0.37 and 0.12 respectively; whereas the profiles of the less reactive BRH and TIR chars observed monotonously decreasing reactivity profile as a function of conversion with the maximum reactivities attained at conversions of < 0.02. The type of reactivity profile observed by the more reactive BW and TRH chars is indicative of a reaction that involves the unblocking of dead pores caused by tar deposition and decomposition and the widening of smaller pores that exposes a larger active surface area to the oxygen during the early stages [57]. The reactivity profile of the less reactive chars on the otherhand, indicate that the amount of reactive surface area decreased with increasing conversion.

The more reactive BW and TRH chars in the combustion tests also exhibited the smallest BET surface areas and largest average pore sizes in the macroporous region. These observations are in agreement with some previous studies investigating coal and biomass char oxidation reactivity where char oxidation was found to occur predominantly through the growth and extension of the meso- and macroporous network with the microporous region remaining relatively unaffected [57,68–70]. In addition to offering improved mass transfer properties by aiding the transport of the reactant and product gases through the char matrix, it is also believed that the surfaces of macropores contain a higher concentration of active sites compared with micropores [68]. This can be rationalised by considering where the different porosity regions occur within the char structure. Micropores are believed to occur predominantly in between highly conjugated, graphene-like crystallite sheets of the char matrix whereas large meso- and macropores are formed at the boundaries of inorganic ash structures and around defects and edges in the graphitic crystallites where most of the oxygen containing functional groups tend to be located [68,71,72].

The propensity of a char to form larger meso- and macro-pores during pyrolysis and oxidation may go some way to explaining the different reactivities; particularly in the case of the BW char which had a considerably larger average pore size (in the macroporous region) and appeared to have the most open structure (Fig. 7). This theory is also likely to explain the lower reactivity of the TIR char which exhibited the opposite morphological traits to the BW char. However the differences in the average pore size and pore size distributions of the rice husk chars is less pronounced. It is therefore more likely that the higher concentration of catalytically active inorganic matter, particularly potassium, present in the TRH was the dominant factor influencing the difference in combustion reactivities of the two rice husks.

The trends in the reactivities of the chars in the CO_2 gasification tests at 1173 K were different to those observed for the combustion tests at 773 K. The reactivity profiles as a function of conversion were also different exhibiting an initial surge in reactivity coinciding with the entry of CO_2 which rapidly decayed to a much lower stable value. This type of reaction profile is characteristic of CO_2-char gasification experiments and is associated with the consumption of organic material at highly active sites within the char matrix [56].

The TIR char was the most reactive char in the CO_2 gasification experiments, with the fast initial reactivity persisting for close to the entire conversion range. The fast and persistent reaction rate is likely due to (i) the improved catalytic activity of certain inorganic constituents (particularly the alkaline earth metals) at the higher temperature; (ii) an improvement in the accessible active surface area due to pore widening and the opening up of previously dead pores as a result of the additional thermal decomposition and pyrolysis at the higher temperatures; and (iii) the high ratio of ash/organic material of the TIR char. During the pre-heating step, the char lost 70 wt% of its organic content such that prior to the CO_2 gasification reaction step, the organic content of the TIR char was 14 wt% compared with 97 wt%, 54 wt% and 46 wt% for the BW, BRH and TRH chars respectively. As a consequence, it is likely that the organic content of the TIR char existed as a disperse, highly active phase on a catalytically-active inorganic ash matrix.

Interestingly, the rice husk chars exhibited significantly lower initial and residual reactivities compared with the BW and TIR chars. The low reactivity is most likely due to increased deactivation and loss of the catalytically active pottassium and sodium containing ash species during heating to 1173 K.

At temperatures of 973–1123 K, potassium in the form of KCl and KOH is lost from the char through vaporisation and at temperatures > 1123 K, K_2CO_3 will decompose [59,72]. K_2CO_3 decomposition will either result in the loss of potassium through the formation of KOH or alternatively the potassium can react with silica to form a deactivated potassium silicate phase. Potassium silicate eutectic melts can form at temperatures as low as 773 K in the presence of Na_2O [73] and is the possible explanation for the appearance of the molten ash coating on the surface of the rice husk chars in the SEM images (Fig. 7). The formation of potassium and other alkali metal silicate phases is exacerbated at high temperatures and in chars containing high concentrations of silica. In addition to deactivating the alkali metal towards char gasification, alkali silicate melts can form an impermeable coating that blocks access to small pores and activated surface sites of the char further impeding char gasification [56,74,75]. A low ash fusion temperature may also lead to other process problems including bed agglomeration and defluidisation in fluidised bed reactors and corrosion due to the acidic nature of the alkali silicates. As a consequence, the potassium concentration of a char becomes less important for gasification reactions at high temperatures; and when present in combination with large amounts of silica, can cause significant inhibition of the char gasification reactivity.

The BW char exhibited the second highest reactivity. The reasonably high reactivity is likely a result of the propensity of the BW char to form macropores and its high concentration of calcium and magnesium compared to the rice husk chars. There is also a clear trend between the combined Ca and Mg content of the chars and the CO_2 gasification reactivities demonstrated by the chars (Fig. 10). Ca and Mg are less susceptible to silicate formation, such that their concentration becomes more important towards char gasification reactivities at the higher temperatures. The lower reactivity compared with the TIR char was likely due to the much lower ratio of organic to ash ratio and lower concentration of alkaline earth metals.

Considering the potential of the different biomass feedstocks as fuels for a gasification process, the results indicate that beech wood would be the most suitable gasifier feed of the four biomass varieties tested in this

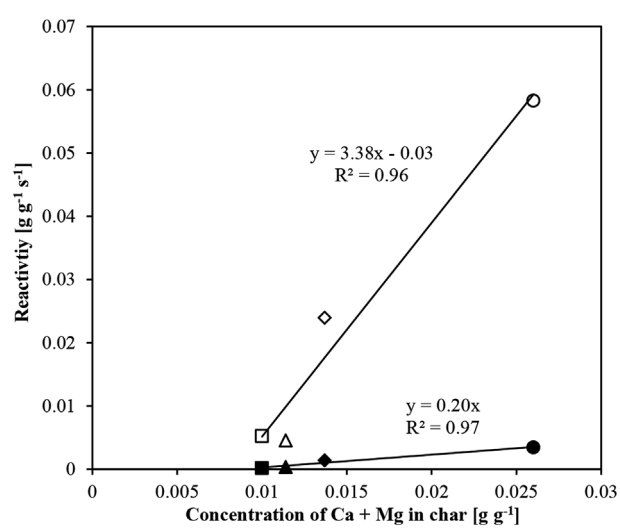

Fig. 10. CO_2 gasification reactivity of the chars generated in the single stage pyrolysis of the different biomass feeds as a function of the char indigenous Ca and Mg concentration. **Experimental Parameters**: ***1st stage***: **Feed** = Variable (1.000 g, 106–150 μm), **carrier gas** = He, **superficial velocity** = 0.1 m s^{-1}, **inlet pressure** = 2.2 bar_a, **heating rate** = 1 K s^{-1}, **hold temperature** = 773 K, **hold time** = 900 s. Maximum initial rate:◇ BW, △BRH, □ TRH, ○ TIR; Rate at X = 0.5 (solid fill).

study. It produced the largest amount of volatiles containing the highest proportions of the combustible gases (CO and CH_4). It also produces the least amount of char, which demonstrated a reasonably high reactivity with both air and CO_2. The large amount of tars initially released by the beech wood during pyrolysis would be largely cracked and reformed in subsequent high temperature gasification and combustion reactions although biomass varieties that release larger amounts of tars during pyrolysis tend to produce gases with a higher tar content when gasified.

Pyrolysis of the two rice husks released similar quantities of volatiles to the beech wood and less tars, however they both had high ash contents and produced chars with low reactivities. If our hypotheses are correct and it is the formation of an ash coating on the surface of the chars inhibiting the reactivity of the chars at the higher temperatures, then it would suggest a gasifier design based on a fluidised-bed reactor would be the optimal system for processing these feedstocks. The abrasive nature of a fluidised bed would act to atrit away the surface of the char exposing new surfaces that could undergo reactions thus enhancing the observed reactivity. However, the low fusion temperature of the ash may cause issues relating to defluidisation of the bed material. Despite the apparent poor performance of these materials, exploitation of this potential energy source is attractive as rice husk is a waste product produced in substantial quantities.

The textile industry residue initially appeared to be the least feasible fuel for gasification. It released the least amount of volatiles and produced the largest amount of char. The char also exhibited the lowest reactivity at 773 K with air. The high sulfur and chlorine contents of 3.99 and 1.65 wt% respectively may further deter the use of this material as a fuel for gasification. However, issues associated with sulfur and chlorine emissions could be abated through blending with other low sulfur and chlorine containing gasifiable waste streams or installation of downstream gas conditioning measures. Furthermore, at 1173 K, the reactivity of the textile industry residue char with CO_2 was significantly higher than any of the other biomass varieties tested in this study. This shows that higher temperatures are necessary for optimal gasification of this feedstock. The high ash content also indicates that a fluidised bed reactor may be most suitable for processing this material particularly if using a larger particle size. Whilst still not the most attractive of feedstocks on account of its low gasifiable organic content, gasification may provide the most efficient method of extracting the energy from this waste feedstock into a convenient fuel gas. This gas (along with the useful heat produced in the gasification process) could then be used to supplement on-site fuel; heat and power use, whilst reducing the size of the waste stream and associated costs of disposal.

3.3. 2-Stage fixed-bed pyrolysis results

3.3.1. Effect of elevated 2nd stage temperature of the tar-cracking product distribution

Two-stage experiments in which the 2nd reactor stage was operated empty at each of the different temperatures was carried out to investigate the effect of elevated temperatures and possible catalytic tar cracking mechanisms on the surface of the Incoloy 800 HT reactor walls [76]. The results from this set of experiments served as a baseline by which to assess the effect of additional cracking mechanisms on the tar and volatile yields caused by the introduction of extra inert surface area (section 3.3.2) and calcined dolomite and limestone (section 3.3.3) into the 2nd stage of the reactor.

Tar yields from beech wood pyrolysis in the two-stage reactor were significantly lower than beech wood pyrolysis in the single stage reactor (Fig. 11). When the 2nd stage was operated at 973 K the amount of tar exiting the reactor was reduced to 26% of the amount exiting the single stage reactor. Further reductions in the tar yield were achieved by increasing the temperature of the 2nd stage up to 1173 K where 97% of the tar was eliminated (Fig. 11).

SEC analysis of the tars exposed to the elevated temperatures of 973 K revealed that the lower molecular mass tar constituents were

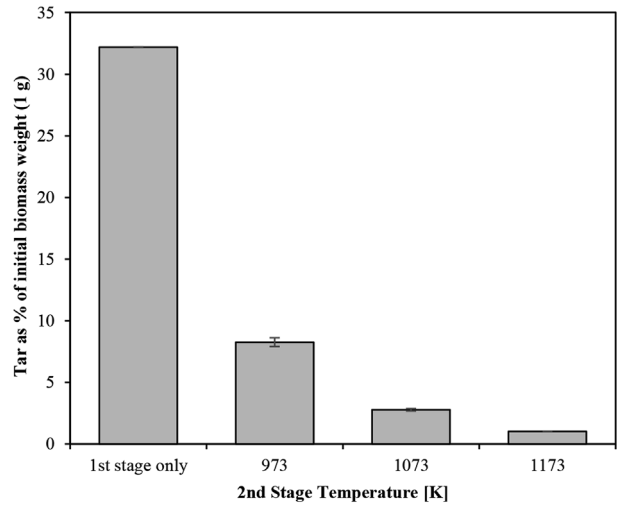

Fig. 11. Tar recovered as a function of 2nd stage temperature. **Experimental Parameters**: ***1st stage***: **Feed** = Beech wood (1.000 g, 106–150 μm), **carrier gas** = He, **superficial velocity** = 0.1 m s^{-1}, **inlet pressure** = 2.2 bar_a, **heating rate** = 1 K s^{-1}, **hold temperature** = 773 K, **hold time** = 900 s. ***2nd stage***: **Bed** = N/A, **superficial velocity** = 0.25 m s^{-1}, **inlet pressure** = 2.1 bar_a, **temperature** = variable.

more susceptible to thermal cracking and possible catalytic cracking on the walls of the Incoloy reactor tube than the higher molecular mass fraction as evidenced by the more intense excluded peak and less intense retained peak compared with the SEC chromatogram of the primary pyrolysis tars generated in the single stage reactor (Fig. 12). The maxima of the peaks for both fractions of the tars generated in the 2-stage reactor at 973 K occurred at shorter elution times indicating an increase in the average molecular mass of both tar fractions compared with the tar generated in the single stage reactor.

The intensity of the excluded peak in the chromatogram of the tars generated at 1073 K decreased back to a similar level to the excluded peak in the chromatogram for the single stage tars, whilst the retained peak became broader and more intense than the equivalent peak in the 973 K tars. The larger width of the retained peak was due to the development of a shoulder that eluted at a similar time to the peak of the retained peak of the 1173 K tars. The elution time of the retained peak was also slightly longer than the equivalent peak in the chromatogram of the 973 K. Increasing the temperature of the 2nd stage to 1173 K caused a further shift in the elution time of the retained peak in the direction of the shoulder of the retained peak in the chromatogram of the 1073 K tars. The retained peak was also more intense and narrower than the equivalent peak in the chromatogram of the 1073 K tars.

These findings indicate that exposing the tars to elevated temperatures of 973–1173 K enhanced the cracking of the larger, high molecular weight tars (as characterised by the excluded peak) into smaller, lighter tar compounds. Increasing the temperature of the 2nd stage also appeared to enhance the cracking of the less thermally stable heavier tars in the lower molecular mass fraction such that the average molecular mass (estimated from the elution time of the retained peak) decreased from 520 u to 400 u and 220 u for 2nd stage temperatures of 973 K, 1073 K and 1173 K respectively. This is also supported by the fact that as the 2nd stage temperature was increased from 1073 K to 1173 K, the retained peak became narrower and more intense corresponding to a decrease in the variety of tar species that have a high enough thermal stability to resist decomposition at 1173 K.

The concentrations of CH_4, CO and CO_2 were also measured in the reactor effluent gas (Fig. 13). CO production increased substantially from 2.9 wt% to 15.5 wt% in the 2-stage reactor at 973 K. Increasing the temperature of 2nd stage to 1073 K and 1173 K resulted in further increases in the amount of CO detected. At a 2nd stage temperature of 1173 K, 22.8 wt% of the initial beech wood feed was converted to CO. The trend in CH_4 production was similar to the trend observed for CO,

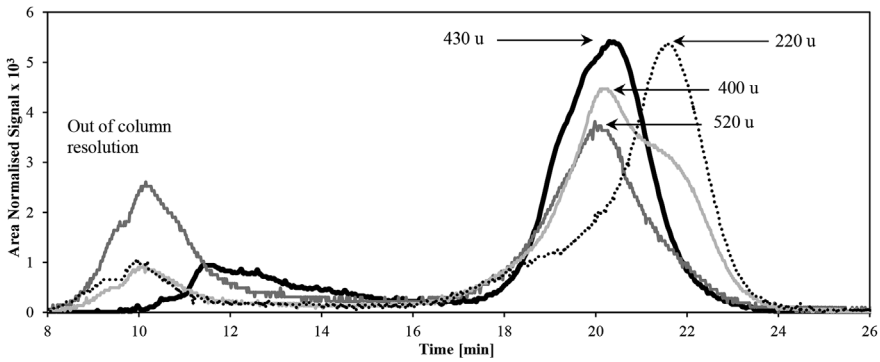

Fig. 12. SEC chromatograms of tars recovered when the temperature of the empty 2nd stage was varied. **Experimental Parameters**: ***1st stage***: **Feed** = Beech wood (1.000 g, 106–150 μm), **carrier gas** = He, **superficial velocity** = 0.1 m s^{-1}, **inlet pressure** = 2.2 bar_a, **heating rate** = 1 K s^{-1}, **hold temperature** = 773 K, **hold time** = 900 s. ***2nd stage***: **Bed** = N/A, **superficial velocity** = 0.25 m s^{-1}, **inlet pressure** = 2.1 bar_a, **temperature** = variable. 1st stage only▬▬▬. 2nd stage temperature = 973 K ▬▬▬, 1073 K ▬▬▬, 1173 K.▪▪▪▪▪▪▪▪▪.

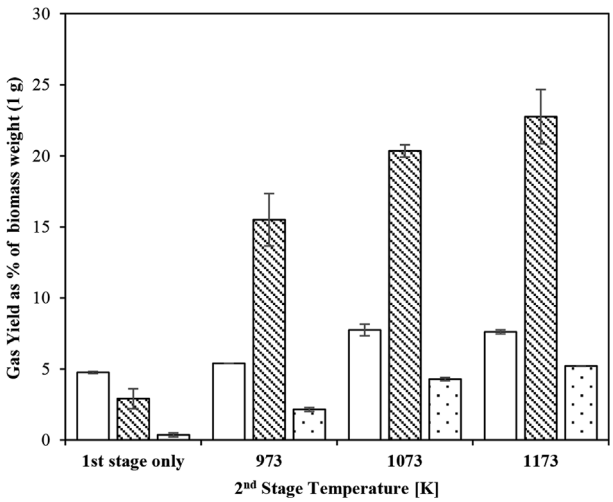

Fig. 13. Gas production as a function of 2nd stage temperature. **Experimental Parameters**: ***1st stage***: **Feed** = Beech wood (1.000 g, 106–150 μm), **carrier gas** = He, **superficial velocity** = 0.1 m s^{-1}, **inlet pressure** = 2.2 bar_a, **heating rate** = 1 K s^{-1}, **hold temperature** = 773 K, **hold time** = 900 s. ***2nd stage***: **Bed** = N/A, **superficial velocity** = 0.25 m s^{-1}, **inlet pressure** = 2.1 bar_a, **temperature** = variable, □ CO; ▨ CH_4; ⊡ CO_2.

however the amount of CH_4 released was much lower.

The total amount of CO_2 produced in the 2-stage reactor at 973 K was similar to the amount released from beech wood pyrolysis in the single stage reactor. A small increase in CO_2 production was detected when the temperature of the 2nd stage was increased from 973 K to 1073 K; however increasing the temperature to 1173 K had no further effect. This suggests that most of the detected CO_2 was produced during pyrolysis and that thermal and catalytic wall tar cracking at elevated temperatures favours the production of the combustible gases CO and CH_4.

3.3.2. The influence of inert surface area on the tar-cracking product distribution

Silica sand beds of varying length (20–40 mm) were introduced into the 2nd reactor stage to investigate the influence of non-reactive surface area on the volatile product distribution of beech wood pyrolysis at 973 K. Sand is inert and has a high thermal capacity; therefore the surface area of the sand remains consistent at high temperatures and does not chemically interact with the pyrolysis products generated in the 1st stage such that only the effect of bed length (i.e. extra inert surface area) on the product distribution was observed. Measurements of the 2nd reactor stage temperature profile revealed that it was parabolic in shape. The central 40 mm section of the 2nd reactor stage was relatively stable (± 12 K at 1173 K). Thus bed lengths were limited to 40 mm to ensure that investigations into bed length and additional inert surface area was conducted under isothermal conditions.

Increasing the inert surface area within the 2nd stage at 973 K did not influence the pyrolysis product distribution further (Table 7). This was also the case when 20 mm sand beds were inserted into the 2nd stage at 1073 K and 1173 K (Fig. 14a) indicating that unstable tar species at the investigated 2nd stage temperatures broke down quickly such that the residence time of the tar species in the empty 2nd stage was sufficient for the thermal and catalytic wall tar cracking reactions to proceed to completion.

3.3.3. The influence of the addition of calcined limestone and dolomite to the 2nd stage sand beds on the tar-cracking product distribution

The presence of both the 20% LS and 20% Dol beds in the 2nd stage caused further reductions in the amounts of tar exiting the reactor (Fig. 14a). The effects were most pronounced at 973 K and 1073 K although this was most likely because 97% of the pyrolysis tars were cracked thermally and on the walls of the reactor at 1173 K. The presence of the 20% LS bed, reduced the tar yield by 25%, 43% and 20% compared to when the reactor was operated with an empty 2nd stage at 973 K, 1073 K and 1173 K respectively. The 20% Dol bed was slightly more effective and caused reductions in the tar yields of 35%, 47% and 40% at 973 K, 1073 K and 1173 K respectively. Increasing the dolomite loading in the bed from 20 wt% to 40 wt% had no further effect (Fig. 14b).

There is little difference between the SEC chromatograms of the tars generated in the reactor packed with the different beds at 973 K (Fig. 15a), indicting that the tar cracking activity of the calcined limestone and dolomite at this temperature was indiscriminate.

Table 7
The effect of different 2nd stage sand bed lengths on the product distribution of beech wood pyrolysis. **Experimental Parameters**: ***1st stage***: **Feed** = Beech wood (1.000 g, 106–150 μm), **carrier gas** = He, **superficial velocity** = 0.1 m s^{-1}, **inlet pressure** = 2.2 bar_a, **heating rate** = 1 K s^{-1}, **hold temperature** = 773 K, **hold time** = 900 s. ***2nd stage***: **Bed** = N/A, **superficial velocity** = 0.25 m s^{-1}, **inlet pressure** = 2.1 bar_a, **temperature** = variable.

2nd stage Bed	Weight as percentage of initial biomass weight (1.000 g)					
	Tars	Chars	CH_4	CO	CO_2	Unidentified
N/A	8.3 ± 0.4	20.7 ± 0.8	2.2 ± 0.4	15.5 ± 1.8	5.4 ± 0	47.9
20 mm sand	8.0 ± 0.6	21.5 ± 1.1	2.3 ± 0.1	16.5 ± 1.1	5.9 ± 0.7	45.8
30 mm sand	7.8 ± 0.4	21.1 ± 1.0	2.2 ± 0.1	15.1 ± 1.8	5.1 ± 0.4	48.7
40 mm sand	8.4 ± 0.2	21.1 ± 1.3	2.2 ± 0	16.9 ± 0.4	4.6 ± 1.1	46.8

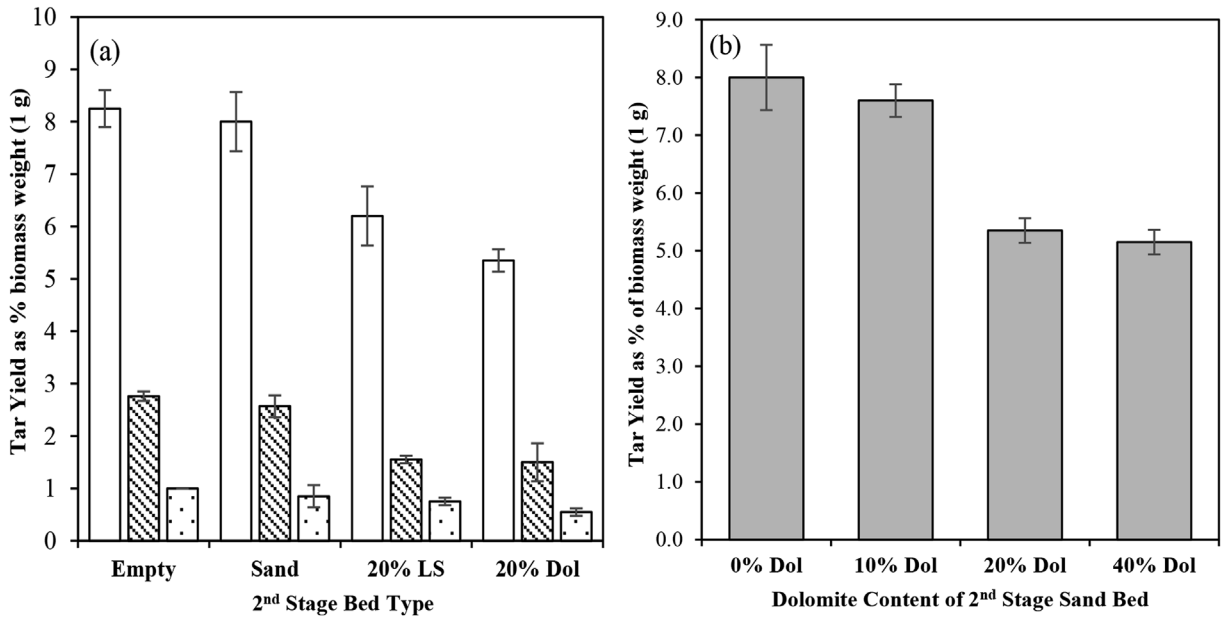

Fig. 14. Tar recovered as (a) a function of 2nd stage bed type and (b) as a function of dolomite loading (0–40 wt%) in the central 10 mm section of a 20 mm 2nd stage sand bed at 973 K. **Experimental Parameters**: ***1st stage***: **Feed** = Beech wood (1.000 g, 106–150 μm), **carrier gas** = He, **superficial velocity** = 0.1 m s^{-1}, **inlet pressure** = 2.2 bar_a, **heating rate** = 1 K s^{-1}, **hold temperature** = 773 K, **hold time** = 900 s. ***2nd stage***: **Bed** = N/A, **superficial velocity** = 0.25 m s^{-1}, **inlet pressure** = 2.1 bar_a, **temperature** = □ 973 K, ▨ 1073 K, ⬚ 1173 K.

However there were differences in the chromatograms of the tars generated in the presence of the different beds at 1073 K and 1173 K.

At 1073 K, the excluded peaks in the chromatogram of tars generated in the presence of the 20% LS and 20% Dol beds were more intense whilst the retained peaks were less intense than the corresponding peaks in the chromatograms of the tars generated in the absence of the catalytic beds (Fig. 15b). This indicates that the presence of calcined limestone and dolomite at 1073 K enhanced the cracking of the lower molecular weight fraction of the tar. Furthermore the retained peak in the chromatogram of the tar generated in the presence of the 20% LS bed had two maxima corresponding to tar species with average molecular masses of 240 u and 400 u. The retention times of these two peaks are both greater than the elution times of the retained peaks in the chromatograms of the tars generated in the presence of the sand bed, the 20% Dol bed and no 2nd stage bed which all elute at the same time and corresponds to an average molecular mass of 410 u. These

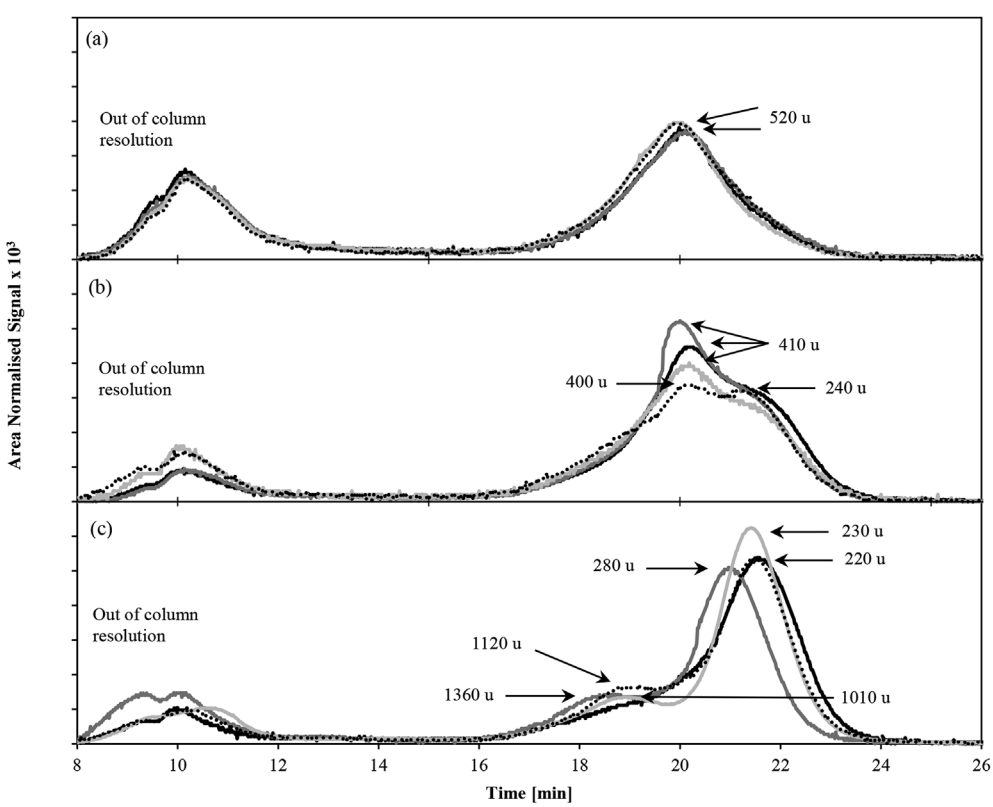

Fig. 15. SEC chromatograms of tars recovered with various beds in the 2nd stage at (a) 973 K, (b) 1073 K, (c) 1173 K. **Experimental Parameters**: ***1st stage***: **Feed** = Beech wood (1.000 g, 106–150 μm), **carrier gas** = He, **inlet pressure** = 2.2 bar_a, **superficial velocity** = 0.1 m s^{-1}, **heating rate** = 1 K s^{-1}, **hold temperature** = 773 K, **hold time** = 1173 K; ***2nd stage***: **inlet pressure** = 2.1 bar_a, **superficial velocity** = 0.25 m s^{-1}, **temperature** = variable, **bed type**: N/A ▬▬; 20 mm sand bed▬▬; 20% LS bed ▬▬; 20% Dol bed.▪▪▪▪▪▪▪▪▪▪.

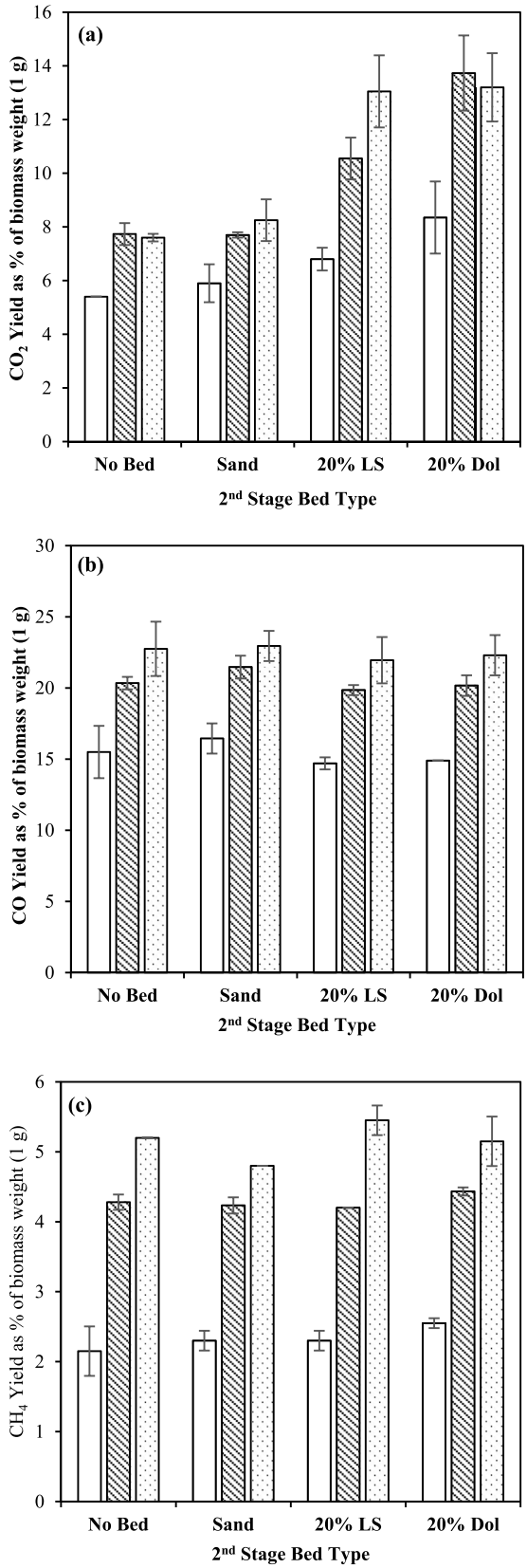

Fig. 16. (a) CO, (b) CH_4 and (c) CO_2 yields after exposure to the different 2nd stage beds. **Experimental Parameters**: ***1st stage***: **Feed** = beech wood (1.000 g, 106–150 μm), **carrier gas** = He, **inlet pressure** = 2.2 bar_a, **superficial velocity** = 0.1 m s^{-1}, **heating rate** = 1 K s^{-1}, **hold temperature** = 773 K, **hold time** = 900 s. ***2nd Stage***: **inlet pressure** = 2.1 bar_a, **superficial velocity** = 0.25 m s^{-1}, **bed** = Variable, **temperature** = □ 973 K, ▨ 1073 K, ⬚ 1173 K.

observations indicate that the presence of calcined limestone at 1073 K enhanced the cracking of the heavier tar species in the lower molecular weight tar fraction which differed from the catalytic activity of the calcined dolomite at this temperature.

SEC analysis of the tars exposed to the different 2nd stage beds at 1173 K also revealed some differences despite there being only very small differences in the tar yields (Fig. 15c). An additional small peak in the chromatograms of the tars exposed to the different beds appeared at elution times of 18–19 min corresponding to the elution of a tar component with an average molecular mass of 1010–1360 u. There were also some differences in the elution times, intensities and ratio of peak areas suggesting that the addition of the different beds had some influence on the tar cracking reaction pathway despite the fact that introducing the beds had little effect on overall tar yield at 1173 K.

The findings from the gas analysis also suggest there may be subtle differences in the tar cracking activities of calcined limestone and dolomite. Although the addition of the different beds did not affect CO and CH_4 production (Fig. 16a and b), CO_2 production was significantly enhanced by the addition of the 20% LS and 20% Dol beds (Fig. 16c). The presence of the 20% LS bed increased CO_2 production by 26%, 38% and 73%, whilst dolomite enhanced CO_2 production by 56%, 78% and 74% at 973 K, 1073 K and 1173 K respectively. CO_2 production in the presence of the 20% LS bed increased with increasing temperature, but decreased in the case of the 20% Dol bed when the temperature was increased from 1073 K to 1173 K. Since both the dolomite and limestone were completely calcined before the pyrolysis experiments were started, the increased production of CO_2 must be a consequence of enhanced tar cracking and possible water-gas shift catalytic activity by the calcined limestone and dolomite in the beds.

The results from the TGA analysis for determining the extent of coke formation on the retrieved limestone and dolomite particles showed that increasing the temperature of the 2nd stage reduced carbon deposition (Table 8). At the temperatures investigated in this work (973–1173 K), coke formation is predominantly caused by decomposition of tars on the surface of the calcined limestone or dolomite particles [77]. The decrease in coke formation with increasing 2nd stage temperature was most likely due to the reduced exposure of the bed material to the tar since more tar would have been cracked before it reached the section of the reactor containing the catalyst beds. Furthermore, the TGA results indicate that whilst limestone was more susceptible to coking than dolomite at 973 K, the reverse was true at 1173 K.

BET analysis revealed that the surface area of the calcined dolomite was significantly larger than the calcined limestone at all the investigated temperatures (Table 9). The larger reactive surface area of the dolomite may explain the higher tar cracking activity of the 20% Dol bed compared to the 20% LS bed. Increasing the temperature enhanced particle sintering which resulted in the observed loss of surface area and corresponding increase in the average pore size diameter for both the limestone and dolomite particles. Increasing the temperature of the 2nd stage also caused the particles to fracture and fragment (Fig. 17). Fragmentation of the dolomite particle was more severe than the limestone particle.

In summary, both calcined dolomite and limestone were shown to

Table 8
Summary of the levels of coking as a percentage of the fully calcined limestone and dolomite particles retrieved from the 20% LS and 20% Dol beds. **Experimental Parameters**: ***1st stage***: **Feed** = beech wood (1.000 g, 106–150 μm), **carrier gas** = He, **inlet pressure** = 2.2 bar_a, **superficial velocity** = 0.1 m s^{-1}, **heating rate** = 1 K s^{-1}, **hold temperature** = 773 K, **hold time** = 900 s. ***2nd Stage***: **inlet pressure** = 2.1 bar_a, **superficial velocity** = 0.25 m s^{-1}, **bed** = Variable, **temperature** = variable.

2nd Stage Temperature	973 K	1073 K	1173 K	
Coking as % of calcined sample weight	Limestone	10%	3%	0%
	Dolomite	6%	3%	2%

Table 9
BET surface areas and BJH average pore diameters for the limestone and dolomite particles retrieved from the 20% LS and 20% Dol beds. **Experimental Parameters**: ***1st stage***: **Feed** = beech wood (1.000 g, 106–150 μm), **carrier gas** = He, **inlet pressure** = 2.2 bar_a, **superficial velocity** = 0.1 m s^{-1}, **heating rate** = 1 K s^{-1}, **hold temperature** = 773 K, **hold time** = 900 s. ***2nd Stage***: **inlet pressure** = 2.1 bar_a, **superficial velocity** = 0.25 m s^{-1}, **bed** = Variable, **temperature** = variable.

2nd Stage Temperature	973 K	1073 K	1173 K
Limestone BET Surface Area [m^2 g^{-1}]	11.59	8.82	4.78
Limestone BJH Average Pore Diameter (1.7–300 nm) [nm]	16.01	20.94	34.68
Dolomite BET Surface Area [m^2 g^{-1}]	23.45	18.62	11.86
Dolomite BJH Average Pore Diameter (1.7–300 nm) [nm]	12.68	13.33	23.27

be effective tar cracking catalysts, however additional measures such as the inclusion of steam or small amounts of O_2 into the gasifier blast gases may be necessary to inhibit coke formation. Alternatively, a periodic regeneration step could be implemented to remove coke build up on the surface of the catalyst and restore the catalytic activity of the material. The propensity of both materials to fragment may also present problems, particularly if employed as a primary catalyst in a fluidised bed gasification environment.

The friability and tendency of these materials to coke may be less problematic for applications as a primary tar cracking catalyst in a dowdraft gasification process where the fluidisability of the material is less important. Such materials could be employed as a single pass catalyst or recycled for multiple passes if the reactor was operated below the slagging (ash-fusion) temperature. There would be no need to separate the catalyst from the ash collected below the grate as the additional mineral content would likely act to enhance the tar cracking activity of the catalyst. The addition of MgO and CaO may provide further benefits in inhibiting the formation of low melting point eutectic salts thereby increasing the temperature range at which the gasifier could be operated under non-slagging conditions. The spent catalyst and ash stream produced from a gasifier fed with agricultural residues could be applied to the fields to aid with mineral content replenishment. Furthermore, MgO and CaO are widely used in agricultural applications as soil additives, fertiliser components, pesticides and contaminated land remediation [78–81].

The findings of this study indicate that both calcined limestone and dolomite are promising materials for in-bed, primary tar cracking catalyst in downdraft gasification applications. Alternatively these materials could be employed as secondary catalysts in a fixed bed guard column downstream of the gasifier where the mechanical stress experienced by the particles could be limited.

4. Summary and conclusions

Four different types of biomass or wastes were pyrolysed in a lab-scale fixed-bed reactor at 773 K. The distribution and nature of the pyrolysis products were determined and analysed. The different biomass varieties were then assessed for applications as fuels for biomass gasification. The product distributions of the three more conventional lignocellulosic biomass varieties produced similar product distributions in terms of their total volatile and char yields although the Thai rice husk produced 40 wt% less tar and more gas than the Brazilian variant. The difference in tar yields was attributed to the higher concentration of potassium present in the Thai rice husk compared with the Brazilian variant and the beech wood. The product distributions and nature of the tars produced from the pyrolysis of beech wood and the Brazilian rice husk appeared to be very similar despite the differences in the O/C ratios, ash content (particularly the inert ash component content), surface area and porosity of the resultant char, indicating that these factors have less influence on biomass pyrolysis behaviour than the concentration of certain catalytically active ash constituents such as potassium.

Pyrolysis of the textile industry solid residue produced the most char and the least amount of volatiles which was attributed to its high ash content and small pores. Small pores impede the release of volatiles from the char matrix while the high ash content provides a larger, potentially catalytically active surface on which secondary tar polymerisation and char forming reactions can take place. Pyrolysis of the textile industry residue produced a tar comprised of lower molecular sized components compared with the other tars. It is possible that the smaller pores of the TIR acted to enhance tar cracking, directing the

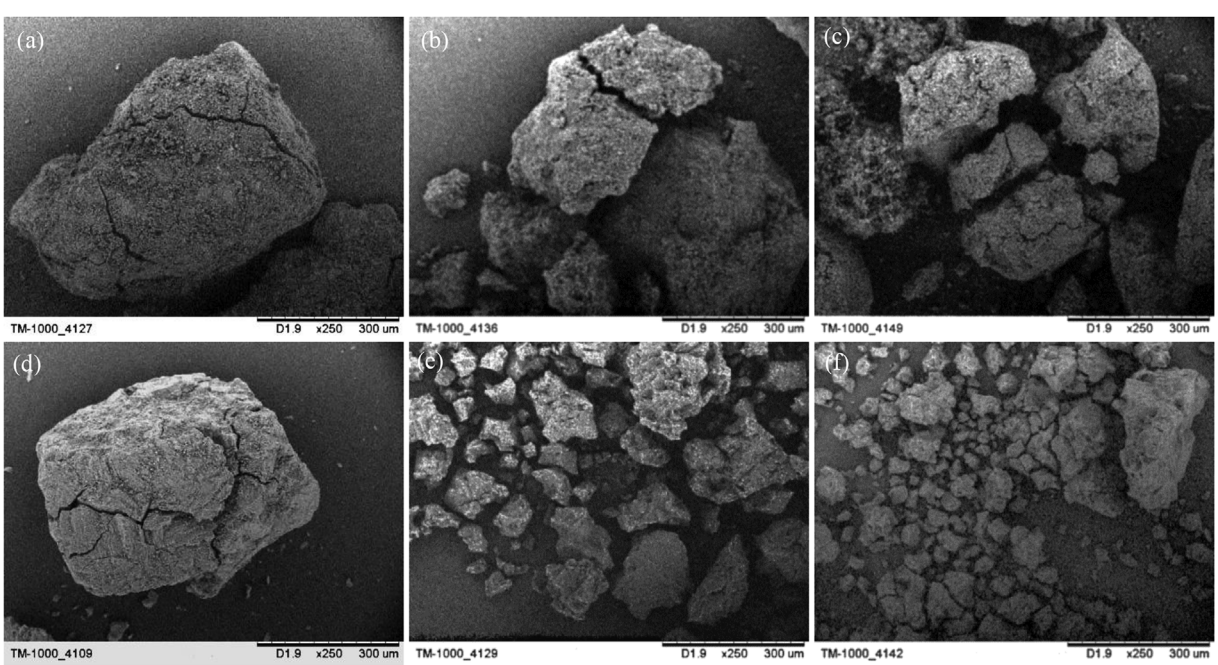

Fig. 17. SEM images of the limestone (a–c) and dolomite particles (d–f) retrieved from the 2nd stage beds after pyrolysis experiments at 973 K (a,d); 1073 K (b,d) and 1173 K (c,f). **Experimental Parameters**: ***1st stage***: **feed** = beech wood (1.000 g, 106–150 μm), **carrier gas** = He, **inlet pressure** = 2.2 bar_a, **superficial velocity** = 0.1 m s^{-1}, **heating rate** = 1 K s^{-1}, **hold temperature** = 973 K, hold time = 900 s. ***2nd stage***: **inlet pressure** = 2.1 bar_a, **superficial velocity** 0.25 m s^{-1}, **bed type** = variable, **temperature** = variable.

formation of lower molecular weight tar components. However, the differences observed in the product distribution and nature of the TIR pyrolysis products may have also been a result of compositional differences between the TIR and the more conventional lignocellulosic biomass varieties and related differences in the thermochemical breakdown pathways.

The resultant pyrolysis chars were further analysed to assess their relative reactivities in air at 773 K and CO_2 at 1173 K. The BW and TRH chars which had the lowest BET surface areas and largest average pore size in the macroporous region, demonstrated the highest reactivity in the air reactivity tests. These findings agree with previous studies that found char oxidation occurs predominantly through the growth and extension of the macroporous network due to their favourable mass transfer characteristics and higher concentration of active sites on the pore surfaces. The high concentration of potassium was also likely to have influenced the high oxidative reactivity of the TRH char compared with the BRH char.

The trends in the gasification reactivity of the char samples when reacted with CO_2 at 1173 K were different. The reactivity of the chars appeared to correlate well with the concentration of Ca and Mg present in the char. Macroporosity and a high ratio of ash to organic content is also likely to have led to enhanced CO_2 gasification reactivity. The chars containing high levels of silica in combination with alkali metals (i.e. the chars derived from the two rice husk samples) demonstrated significantly lower reactivities which were attributed to the formation of molten alkali silicate phases that were likely to have deactivated the catalytic effect of the alkali metal and blocked access to the pores reducing the available reactive surface area.

In the second section of this work, the fixed-bed reactor in its two-stage configuration was utilised to investigate the effect of temperature, surface area and presence of potential catalytically active materials on the pyrolysis product distribution of a beech wood biomass fuel. Subjecting the tars to higher temperatures caused a significant reduction in the amount of tars collected. 97% of the primary tars released in the first stage pyrolysis were cracked in the 2nd stage at 1173 K. Tar cracking favoured the production of CO with yields of 22.2 wt% measured at 1173 K. Increasing the surface area in the 2nd stage by inserting sand beds had no additional effect on the product distribution.

The presence of sand beds containing calcined limestone or dolomite in the 2nd stage of the reactor further enhanced tar cracking. The effects were most pronounced at 973 K and 1073 K where the presence of the bed containing calcined limestone reduced tars by 25% and 43% compared with the equivalent tar yields from the reactor with an empty 2nd stage. The addition of calcined dolomite to the sand beds was slightly more effective than the addition of calcined limestone and reduced the tar yield by 35% and 47% at 973 K and 1073 K respectively. At 1173 K, 98% of the primary pyrolysis tar was eliminated after exposure to the bed containing calcined dolomite. The slightly greater reactivity of dolomite was attributed to its higher surface area. In summary, both calcined dolomite and limestone demonstrated significant promise for applications as in-bed primary tar cracking catalysts for downdraft gasification applications.

Acknowledgements

The authors wish to thank the EPSRC under the RCUK Energy programme for MBH's PhD studentship and additional funding under EP/I010912/1. Multi-scale evaluation of advanced technologies for capturing the CO_2: chemical-looping applied to solid fuels. Data related to the study may be requested through https://www.imperial.ac.uk/people/p.fennell.

References

[1] M.F. Demirbaş, M. Balat, H. Balat, Potential contribution of biomass to the sustainable energy development, Energy Conv. Manag. 50 (7) (2009) 1746–1760.
[2] T.B. Reed, A. Das, Handbook of Biomass Downdraft Gasifier Engine Systems, Biomass Energy Foundation, 1988.
[3] T.A. Milne, N. Abatzoglou, R.J. Evans, Biomass Gasifier "tars": Their Nature, Formation, and Conversion, National Renewable Energy Laboratory Golden, CO, 1998.
[4] L. Devi, K.J. Ptasinski, F. Janssen, A review of the primary measures for tar elimination in biomass gasification processes, Biomass Bioenerg. 24 (2) (2003) 125–140.
[5] R. Warnecke, Gasification of biomass: comparison of fixed bed and fluidized bed gasifier, Biomass Bioenerg. 18 (6) (2000) 489–497.
[6] C.Z. Wu, H. Huang, S.P. Zheng, X.L. Yin, An economic analysis of biomass gasification and power generation in China, Bioresour. Technol. 83 (1) (2002) 65–70.
[7] R. Banerjee, Comparison of options for distributed generation in India, Energy Policy 34 (1) (2006) 101–111.
[8] J. Han, H. Kim, The reduction and control technology of tar during biomass gasification/pyrolysis: an overview, Renew. Sustain. Energy Rev. 12 (2) (2008) 397–416.
[9] S. Anis, Z.A. Zainal, Tar reduction in biomass producer gas via mechanical, catalytic and thermal methods: a review, Renew. Sustain. Energy Rev. 15 (5) (2011) 2355–2377.
[10] V.S. Sikarwar, M. Zhao, P. Clough, J. Yao, X. Zhong, M.Z. Memon, N. Shah, E.J. Anthony, P.S. Fennell, An overview of advances in biomass gasification, Energy & Environ. Sci. 9 (10) (2016) 2939–2977.
[11] K. Tomishige, T. Miyazawa, M. Asadullah, S.I. Ito, K. Kunimori, Catalyst performance in reforming of tar derived from biomass over noble metal catalysts, Green Chem. 5 (4) (2003) 399–403.
[12] R. Zhang, Y. Wang, R.C. Brown, Steam reforming of tar compounds over Ni/olivine catalysts doped with CeO_2, Energy Conv. Manag. 48 (1) (2007) 68–77.
[13] C. Li, D. Hirabayashi, K. Suzuki, Development of new nickel based catalyst for biomass tar steam reforming producing H_2-rich syngas, Fuel Process. Technol. 90 (6) (2009) 790–796.
[14] F.L. Chan, A. Tanksale, Review of recent developments in Ni-based catalysts for biomass gasification, Renew. Sustain. Energy Rev. 38 (2014) 428–438.
[15] Y.F. Shen, P.T. Zhao, Q.F. Shao, D.C. Ma, F. Takahashi, K. Yoshikawa, In-situ catalytic conversion of tar using rice husk char-supported nickel-iron catalysts for biomass pyrolysis/gasification, Appl. Catal. B-Environ 152 (2014) 140–151.
[16] A. Orío, J. Corella, I. Narváez, Performance of different dolomites on hot raw gas cleaning from biomass gasification with air, Ind. Eng. Chem. Res. 36 (9) (1997) 3800–3808.
[17] J.F. González, S. Román, G. Engo, J.M. Encinar, G. Martínez, Reduction of tars by dolomite cracking during two-stage gasification of olive cake, Biomass Bioenerg. 35 (10) (2011) 4324–4330.
[18] C. Berrueco, D. Montane, B.M. Güell, G. del Alamo, Effect of temperature and dolomite on tar formation during gasification of torrefied biomass in a pressurized fluidized bed, Energy 66 (2014) 849–859.
[19] J. Delgado, M.P. Aznar, J. Corella, Calcined dolomite, magnesite, and calcite for cleaning hot gas from a fluidized bed biomass gasifier with Steam: life and usefulness, Ind. Eng. Chem. Res. 35 (10) (1996) 3637–3643.
[20] M. Siedlecki, R. Nieuwstraten, E. Simeone, W. de Jong, A.H.M. Verkooijen, Effect of magnesite as bed material in a 100 kWth Steam – Oxygen blown circulating fluidized-bed biomass gasifier on gas composition and tar formation, Energy & Fuels 23 (11) (2009) 5643–5654.
[21] A. Erkiaga, G. Lopez, M. Amutio, J. Bilbao, M. Olazar, Steam gasification of biomass in a conical spouted bed reactor with olivine and gamma-alumina as primary catalysts, Fuel Process. Technol. 116 (2013) 292–299.
[22] M. Virginie, J. Adánez, C. Courson, L.F. de Diego, F. García-Labiano, D. Niznansky, A. Kiennemann, P. Gayán, A. Abad, Effect of Fe-olivine on the tar content during biomass gasification in a dual fluidized bed, Appl. Catal. B-Environ 121 (2012) 214–222.
[23] F. Miccio, B. Piriou, G. Ruoppolo, R. Chirone, Biomass gasification in a catalytic fluidized reactor with beds of different materials, Chem. Eng. J. 154 (1) (2009) 369–374.
[24] J. Gil, M.A. Caballero, J.A. Martín, M.-P. Aznar, J. Corella, Biomass gasification with air in a fluidized bed: effect of the in-bed use of dolomite under different operation conditions, Ind. Eng. Chem. Res. 38 (11) (1999) 4226–4235.
[25] I. Narváez, A. Orío, M.P. Aznar, J. Corella, Biomass gasification with air in an atmospheric bubbling fluidized bed. Effect of six operational variables on the quality of the produced raw gas, Ind. Eng. Chem. Res. 35 (7) (1996) 2110–2120.
[26] L. Wei, S. Xu, L. Zhang, C. Liu, H. Zhu, S. Liu, Steam gasification of biomass for hydrogen-rich gas in a free-fall reactor, Int. J. Hydrog. Energy 32 (1) (2007) 24–31.
[27] P.A. Simell, J.O. Hepola, A.O.I. Krause, Effects of gasification gas components on tar and ammonia decomposition over hot gas cleanup catalysts, Fuel 76 (12) (1997) 1117–1127.
[28] J. Delgado, M.P. Aznar, J. Corella, Biomass gasification with steam in fluidized Bed: effectiveness of CaO, MgO, and CaO – MgO for hot raw gas cleaning, Ind. Eng. Chem. Res. 36 (5) (1997) 1535–1543.
[29] J. Corella, J.M. Toledo, R. Padilla, Olivine or dolomite as in-bed additive in biomass gasification with air in a fluidized Bed: which is better? Energy & Fuels 18 (3) (2004) 713–720.
[30] S. Rapagnà, N. Jand, A. Kiennemann, P.U. Foscolo, Steam-gasification of biomass in a fluidised-bed of olivine particles, Biomass Bioenergy 19 (3) (2000) 187–197.
[31] S. Koppatz, C. Pfeifer, R. Rauch, H. Hofbauer, T. Marquard-Moellenstedt, M. Specht, H_2 rich product gas by steam gasification of biomass with in situ CO2 absorption in a dual fluidized bed system of 8 MW fuel input, Fuel Process. Technol. 90 (7) (2009) 914–921.
[32] L. Devi, K.J. Ptasinski, F.J.J.G. Janssen, S.V.B. van Paasen, P.C.A. Bergman,

J.H.A. Kiel, Catalytic decomposition of biomass tars: use of dolomite and untreated olivine, Renew. Energy 30 (4) (2005) 565–587.
[33] R. Kandiyoti, A.A. Herod, K.D. Bartle, T.J. Morgan, Solid Fuels and Heavy Hydrocarbon Liquids: Thermal Characterization and Analysis, second ed., Elsevier Science Pub., Amsterdam Oxford London New York, 2017.
[34] Y. Huang, X. Yin, C. Wu, C. Wang, J. Xie, Z. Zhou, L. Ma, H. Li, Effects of metal catalysts on CO_2 gasification reactivity of biomass char, Biotechnol. Adv. 27 (5) (2009) 568–572.
[35] N.H. Florin, A.T. Harris, Mechanistic study of enhanced H_2 synthesis in biomass gasifiers with in-situ CO_2 capture using CaO, Aiche J. 54 (4) (2008) 1096–1109.
[36] N. Armbrust, G. Duelli, H. Dieter, G. Scheffknecht, Calcium looping cycle for hydrogen production from biomass gasification syngas: experimental investigation at a 20 kWth dual fluidized-bed facility, Ind. Eng. Chem. Res. 54 (21) (2015) 5624–5634.
[37] B.-M. Steenari, A. Lundberg, H. Pettersson, M. Wilewska-Bien, D. Andersson, Investigation of ash sintering during combustion of agricultural residues and the effect of additives, Energy & Fuels 23 (11) (2009) 5655–5662.
[38] C. Bolton, C.E. Snape, R.J. Obrien, R. Kandiyoti, Influence of carrier gas-flow and heating rates in fixed-bed hydropyrolysis of coal, Fuel 66 (10) (1987) 1413–1417.
[39] R.V. Pindoria, J.-Y. Lim, J.E. Hawkes, M.-J. Lazaro, A.A. Herod, R. Kandiyoti, Structural characterization of biomass pyrolysis tars/oils from eucalyptus wood waste: effect of H_2 pressure and sample configuration, Fuel 76 (11) (1997) 1013–1023.
[40] A.G. Collot, Y. Zhuo, D.R. Dugwell, R. Kandiyoti, Co-pyrolysis and co-gasification of coal and biomass in bench-scale fixed-bed and fluidised bed reactors, Fuel 78 (6) (1999) 667–679.
[41] S. Monteiro Nunes, N. Paterson, D.R. Dugwell, R. Kandiyoti, Tar formation and destruction in a simulated downdraft, fixed-bed Gasifier: reactor design and initial results, Energy & Fuels 21 (5) (2007) 3028–3035.
[42] S. Monteiro Nunes, N. Paterson, A. Herod, D. Dugwell, R. Kandiyoti, Tar formation and destruction in a fixed bed reactor simulating downdraft gasification: optimization of conditions, Energy & Fuels 22 (3) (2008) 1955–1964.
[43] F. Dabai, N. Paterson, M. Millan, P. Fennell, R. Kandiyoti, Tar formation and destruction in a fixed-bed reactor simulating downdraft gasification: equipment development and characterization of tar-cracking products, Energy & Fuels 24 (2010) 4560–4570.
[44] F. Dabai, N. Paterson, M. Milian, P. Fennell, R. Kandiyoti, Tar formation and destruction in a fixed bed reactor simulating downdraft gasification: effect of reaction conditions on tar cracking products, Energy & Fuels 28 (3) (2014) 1970–1982.
[45] A.A. Herod, Y. Zhuo, R. Kandiyoti, Size-exclusion chromatography of large molecules from coal liquids, petroleum residues, soots, biomass tars and humic substances, J. Biochem. Biophysical Methods 56 (1–3) (2003) 335–361.
[46] M. Asif, S.J. Parry, Elimination of reagent blank problems in the fire-assay preconcentration of the platinum group elements and gold with a nickel sulfide bead of less than one gram mass, Analyst 114 (1989) 1057–1059.
[47] R. Zanzi, K. Sjöström, E. Björnbom, Rapid pyrolysis of agricultural residues at high temperature, Biomass Bioenergy 23 (5) (2002) 357–366.
[48] R.H. Venderbosch, W. Prins, Fast pyrolysis technology development, Biofuels, Bioprod. Biorefining 4 (2) (2010) 178–208.
[49] M. Nik-Azar, M.R. Hajaligol, M. Sohrabi, B. Dabir, Mineral matter effects in rapid pyrolysis of beech wood, Fuel Process. Technol. 51 (1) (1997) 7–17.
[50] R.J.M. Westerhof, H.S. Nygård, W.P.M. van Swaaij, S.R.A. Kersten, D.W.F. Brilman, Effect of particle geometry and microstructure on fast pyrolysis of beech wood, Energy & Fuels 26 (4) (2012) 2274–2280.
[51] Y. Somrang, Effect of Operating Conditions on Product Distributions and Bio-oil Ageing in Biomass Pyrolysis, PhD Thesis Imperial College London, UK, 2012.
[52] W.T. Tsai, M.K. Lee, Y.M. Chang, Fast pyrolysis of rice husk: product yields and compositions, Bioresour. Technol. 98 (1) (2007) 22–28.
[53] Y. Qian, J. Zhang, J. Wang, Pressurized pyrolysis of rice husk in an inert gas sweeping fixed-bed reactor with a focus on bio-oil deoxygenation, Bioresour. Technol. 174 (Supplement C) (2014) 95–102.
[54] S. Yaman, Pyrolysis of biomass to produce fuels and chemical feedstocks, Energy Conv. Manag. 45 (5) (2004) 651–671.
[55] K. Raveendran, A. Ganesh, K.C. Khilar, Influence of mineral matter on biomass pyrolysis characteristics, Fuel 74 (12) (1995) 1812–1822.
[56] M.P. Kannan, G.N. Richards, Gasification of biomass chars in carbon dioxide: dependence of gasification rate on the indigenous metal content, Fuel 69 (6) (1990) 747–753.
[57] O. Senneca, Kinetics of pyrolysis, combustion and gasification of three biomass fuels, Fuel Process. Technol. 88 (1) (2007) 87–97.
[58] W. Degroot, T.H. Osterheld, G.N. Richards, The influence of natural and added catalysts in the gasification of wood chars, in: A.V. Bridgwater, J.L. Kuester (Eds.), Research in Thermochemical Biomass Conversion, Springer, Netherlands, 1988, pp. 327–341.
[59] A.V. Bridgwater, Progress in Thermochemical Biomass Conversion, John Wiley & Sons, London, 2008.
[60] H. Yang, R. Yan, H. Chen, C. Zheng, D.H. Lee, D.T. Liang, In-depth investigation of biomass pyrolysis based on three major Components: hemicellulose, cellulose and lignin, Energy & Fuels 20 (1) (2006) 388–393.
[61] K. Raveendran, A. Ganesh, K.C. Khilar, Pyrolysis characteristics of biomass and biomass components, Fuel 75 (8) (1996) 987–998.
[62] K. Raveendran, A. Ganesh, Adsorption characteristics and pore-development of biomass-pyrolysis char, Fuel 77 (7) (1998) 769–781.
[63] A.V. Bridgwater, D. Meier, D. Radlein, An overview of fast pyrolysis of biomass, Org. Geochem. 30 (12) (1999) 1479–1493.
[64] C. Philpot, Influence of mineral content on the pyrolysis of plant materials, For. Sci. 16 (4) (1970) 461–471.
[65] A. Jensen, K. Dam-Johansen, M.A. Wójtowicz, M.A. Serio, Tg-ftir study of the influence of potassium chloride on wheat straw pyrolysis, Energy & Fuels 12 (5) (1998) 929–938.
[66] T.J. Morgan, S.Q. Turn, A. George, Fast pyrolysis behavior of banagrass as a function of temperature and volatiles residence time in a fluidized bed reactor, PLoS One 10 (8) (2015) e0136511.
[67] T.J. Morgan, S.Q. Turn, N. Sun, A. George, Fast pyrolysis of tropical biomass species and influence of water pretreatment on product distributions, PLoS One 11 (3) (2016) e0151368.
[68] R.H. Hurt, A.F. Sarofim, J.P. Longwell, The role of microporous surface area in the gasification of chars from a sub-bituminous coal, Fuel 70 (9) (1991) 1079–1082.
[69] I. Aarna, E.M. Suuberg, Changes in reactive surface area and porosity during char oxidation, Symposium Int. Combust. 27 (2) (1998) 2933–2939.
[70] C. Fushimi, K. Araki, Y. Yamaguchi, A. Tsutsumi, Effect of heating rate on steam gasification of biomass. 1. Reactivity of char, Ind. Eng. Chem. Res. 42 (17) (2003) 3922–3928.
[71] J. Lehmann, S. Joseph, Biochar for Environmental Management: Science and Technology, Routledge, 2012.
[72] P.A. Jensen, F. Frandsen, K. Dam-Johansen, B. Sander, Experimental investigation of the transformation and release to gas phase of potassium and chlorine during straw pyrolysis, Energy & Fuels 14 (6) (2000) 1280–1285.
[73] A. Pelton, M. Blander, Thermodynamic analysis of ordered liquid solutions by a modified quasichemical approach- Application to silicate slags, MTB 17 (4) (1986) 805–815.
[74] L.H. Sørensen, J.S. Fjellerup, U.B. Henriksen, A. Moilanen, E. Winther, An Evaluation of Char Reactivity and Ash Properties in Biomass Gasification: Fundamental Processes in Biomass Gasification, ReaTech, Germany, 2000.
[75] A. Moilanen, Thermogravimetric Characterisations of Biomass and Waste for Gasification Processes, PhD Thesis VTT Technical Research Centre, Finland, 2006.
[76] F. Bustamante, R.M. Enick, R.P. Killmeyer, B.H. Howard, K.S. Rothenberger, A.V. Cugini, B.D. Morreale, M.V. Ciocco, Uncatalyzed and wall-catalyzed forward water-gas shift reaction kinetics, Aiche J. 51 (5) (2005) 1440–1454.
[77] T. Mendiara, J.M. Johansen, R. Utrilla, P. Geraldo, A.D. Jensen, P. Glarborg, Evaluation of different oxygen carriers for biomass tar reforming (I): carbon deposition in experiments with toluene, Fuel 90 (3) (2011) 1049–1060.
[78] R.J. Haynes, R. Naidu, Influence of lime, fertilizer and manure applications on soil organic matter content and soil physical conditions: a review, Nutrient Cycl. Agroecosyst. 51 (2) (1998) 123–137.
[79] M. Puschenreiter, O. Horak, W. Friesl, W. Hartl, Low-cost agricultural measures to reduce heavy metal transfer into the food chain–a review, Plant Soil Environ. 51 (1) (2005) 1–11.
[80] M. Sceats, Oxide products formed from calcined carbonate powder for use as biocide, chemical detoxifier and catalyst support products, Google Pat., 2015.
[81] M. Sceats, P. Hodgson, Improved pathogen inhibitor, world wide patent WO2016112425 A1 (2016).